

Cite this: *Mater. Adv.*, 2025,  
6, 4174Received 1st February 2025,  
Accepted 30th April 2025

DOI: 10.1039/d5ma00090d

rsc.li/materials-advances

# A review of core–shell metal–organic frameworks: preparation and biomedical applications

Simindokht Zarei-Shokat, Sheyda Abedi-Banaei, Amir Kashtiaray, Zahra Yazdi,  
Haniyehalsadat Amirhosseini and Ali Maleki \*

Core–shell metal–organic frameworks (MOFs) are an advanced class of hybrid materials, and their synthesis methods are crucial for determining their functionality in biomedical applications. Various synthetic strategies have been developed to create these hierarchical structures, each offering unique advantages in controlling shell thickness, core composition, crystallinity, and surface properties. Recent advancements in preparing core–shell MOF structures have focused on developing composite structures that involve MOFs integrated with other materials, such as nanoparticles, metal sulfides, and metal oxides. In this context, we explore different classes of core@MOF, MOF@shell, and MOF@MOF structures. Additionally, we discuss the practical applications of core–shell MOFs in anti-cancer and antibacterial activities, bioimaging, biosensing, and synergistic therapy, as well as their therapeutic potential.

## 1. Introduction

“Similar microporous structures zeolite but using organic building blocks and metal have the potential for more precise

rational design by controlling the shape, size, and functionalization of the pores. We are announcing the creation of MOFs intended to selectively bind aromatic guest molecules”. This is the initial description of the MOF structure by Yaghi in 1995.<sup>1</sup> Interest in this area was sparked in the late 1999 when Yaghi *et al.* synthesized their MOFs based on the concept of reticular design and named MOF-5, also known as IRMOF-1; the compound has the formula  $Zn_4O(BDC)_3$  and is a cubic MOF,

*Catalysts and Organic Synthesis Research Laboratory, Department of Chemistry, Iran University of Science and Technology, Tehran 16846-13114, Iran.*  
E-mail: maleki@iust.ac.ir

**Simindokht Zarei-shokat**

Simindokht Zarei-Shokat was born in May 1996 in Damghan, Iran (Islamic Republic), and completed her education at Sampad High School (Damghan) in the Experimental Sciences. She graduated from the University of Damghan (DU) with a BSc (2019) in applied chemistry. Then, she continued her study in the field of nanochemistry as an MSc student in the chemistry department of Iran University of Science & Technology (IUST) (started in October 2019). Currently, she is a PhD student at the Institute for NanoScience and NanoTechnology, Sharif University of Technology, majoring in nanotechnology. Also, she is working on different projects as a senior researcher under the supervision of Prof. Ali Maleki at IUST right now and her research interest focuses on drug delivery and cancer therapy.

**Sheyda Abedi-banaei**

Sheyda Abedi-banaei was born in April 2001 in Tehran, Iran (Islamic Republic). She graduated from the University Islamic Azad South Tehran Branch Faculty of Engineering (2023) in applied chemistry. Currently, she is an MSc student in Organic chemistry at Iran University of Science & Technology (IUST) (started in October 2023). Also, she is working on different projects as a researcher under the supervision of Prof. Ali Maleki at IUST right now and her research interest focuses on drug delivery.



representing the start of this type of material's history.<sup>2</sup> MOFs are remarkable organic–inorganic hybrid compounds characterized by one-, two-, or three-dimensional (1D, 2D, and 3D) structural topologies. Composed of inorganic metal ions or clusters alongside organic ligands, MOFs exhibit exceptional properties, such as high surface area, micro- and mesoporosity, and significant potential for further chemical functionalization.<sup>3</sup> Their applicability in the biomedical sector has surged in recent years, solidifying MOFs as a pivotal component in advancing innovative solutions.<sup>4</sup> Core–shell structures have attracted considerable interest because of their distinct characteristics and

varied compositions, and the core–shell MOF includes three structures: core@MOF, MOF@shell, and MOF@MOF.<sup>4</sup> The core and the shell can consist of silica,<sup>5</sup> polymers,<sup>6,7</sup> nanoparticles,<sup>8</sup> quantum dots (BQ),<sup>9</sup> carbon materials,<sup>8</sup> and MOFs,<sup>6</sup> which act as either shells or cores. The distinctive structure of core–shell MOFs consists of a functional core encased by a specialized shell, offering numerous synergistic advantages. Conventional MOFs frequently experience structural instability when exposed to aqueous environments or biological fluids.<sup>10</sup> In contrast, the shell surrounding core–shell MOFs serves as a protective barrier, preventing early degradation of the core and preserving structural



**Amir Kashtiaray**

*Amir Kashtiaray was born in Tehran in 1988. He graduated from Payame Noor University (PNT) with a BSc (2011). Then, he continued his academic study as an MSc Student in Analytical Chemistry at the Iran University of Science and Technology (IUST) and graduated in 2020. His achievements include more than 50 inventions, several gold and silver medals awarded from the World Invention Exhibition, in addition to special prizes and 13 diplomas.*

*Amir was introduced as the best inventor by different countries' invention academies in 2010 and 2011. Several ISI publications are also another honor for him. He is the CEO of Kashtiaray Nano Technology (Founded by Amir in 2017). Currently, he is working on different projects at IUST as a Senior Researcher focusing on drug development, drug delivery, high-tech pharmaceutical compounds, hyphenated techniques in chromatography, and advanced methods in microextraction and sample preparation.*



**Zahra Yazdi**

*Zahra Yazdi was born in November 1998 in Tehran. She completed secondary school at Shahideh Dokhanchi School (Tehran) in the experimental field. She graduated from South Tehran University (Tehran) with a bachelor's degree in applied chemistry. Also, due to her great interest in chemistry and pharmaceuticals, she worked as an intern at Kharazmi Pharmaceuticals and for some time in the Pharmaceutical Synthesis Research Department at Tehran University.*

*She is currently doing research in the field of drug delivery in the master's degree in the field of nanochemistry, under the supervision of Prof. Ali Maleki.*



**Haniyehalsadat Amirhosseini**

*Haniyehalsadat Amirhosseini was born in March 1999 in Damghan and completed her education at Sampad High School (2018) in Experimental Sciences. She graduated from Damghan University (DU) with a BSc (2022) in Applied Chemistry. Then, she continued her study in nanochemistry as an MSc student in the Chemistry Department of Iran University of Science & Technology (IUST) (started in October 2022) under the supervision of Prof. Ali Maleki.*

*Currently, she is working on different projects as a researcher at IUST and her research interest focuses on nanomaterials and their biomedical and environmental applications.*



**Ali Maleki**

*Prof. Dr Ali Maleki was born in Mianeh, East Azerbaijan in 1980. He received his PhD in Chemistry in 2009. He started his career as an Assistant Professor at the Iran University of Science and Technology (IUST) in 2010, where he is currently a Full Professor. His research interests focus on the design and development of novel catalysts, nanomaterials, and green chemistry. He has hundreds of ISI-JCR publications. Some of his honors include Distinguished*

*Researcher of IUST in the period 2010–2025, IUPAC Prize for Green Chemistry in 2016, and Top 1% International Scientists in ESI (Web of Science) in 2018–2024.*



integrity under physiological conditions, such as fluctuating pH levels or the presence of enzymes. Furthermore, the shell layer can be tailored to respond to specific biological triggers, like pH changes, redox conditions, or enzymes, facilitating site-specific and on-demand drug release.<sup>11,12</sup> Applying a biocompatible shell such as a zeolitic imidazolate framework (ZIF), a polymer coating, or silica can reduce potential toxic interactions, improving tolerability and safety profiles *in vivo*. Core-shell designs can also incorporate multiple functions within a single system. For instance, the core can act as a storage reservoir for drug molecules, while the shell can include imaging agents (such as  $Gd^{3+}$  for MRI or fluorescent dyes), targeting ligands, or responsive components.<sup>13–15</sup> This multifunctionality supports theranostic applications, merging diagnostics and therapy into one delivery system. In summary, core-shell MOFs offer a customizable, multi-layered platform that overcomes the limitations of traditional MOFs.<sup>16–19</sup> In 2007, William *et al.* were the first to describe a core-shell structure using nanoscale metal-organic frameworks (NMOFs) and silica. In this structure, the NMOFs, serving as the core, consisted of an  $Ln(BDC)1.5(H_2O)_2$  composition, where Ln represents  $Eu^{3+}$ ,  $Gd^{3+}$ , or  $Tb^{3+}$  and BDC stands for 1,4-benzenedicarboxylate. The silica formed the shell around the core, highlighting the central role of NMOFs in this structure.<sup>20</sup> The methods for creating core-shell structures differ because of their diverse range and various uses. According to the latest research advancements, the methods for creating core-shell MOFs can be grouped into multiple classifications: surface modification methods, post-modification methods, *in situ* growth methods, self-template sacrifice methods, epitaxial growth methods, and one-pot methods. Various techniques have been explored for producing core-shell MOFs and their composite formations. The *in situ* growth method, with its more straightforward preparation process, presents a challenge in achieving a consistent coating of the external MOF shell onto the internal core. The selection of each method is of utmost importance, as it is guided by the specific needs and circumstances in which the framework will be employed, and can significantly impact the outcome of the work.<sup>21</sup> The core-shell MOF's design boasts an extensive specific surface area and a high pore volume, making it incredibly versatile. The pore size can be easily customized to fit various needs and allows for rapid cargo transfer and diffusion. Plus, with its exceptional biocompatibility and biodegradability, this structure stands out as a sustainable choice for different applications. Moreover, it demonstrates the structural benefits of multiple characteristics, including a roomy cavity, substantial loading capacity, and protective properties. As a result, core-shell MOFs are considered ideal materials for biomedical applications.<sup>22</sup> This article will discuss the latest progress in core-shell MOF materials, covering their production, modification, and medical uses like delivering drugs, monitoring biological processes, imaging, and treating cancer. Core-shell MOFs present exciting opportunities in drug delivery by encapsulating therapeutic molecules through methods like pore encapsulation, covalent binding, and surface adsorption. Utilizing van der Waals forces, electrostatic interactions,  $\pi$ - $\pi$  stacking, and hydrogen bonding, these frameworks effectively transport and release

medications. These materials are suitable for drug delivery and are not only non-responsive to stimuli but also responsive to various stimuli, including pH, magnetic field, light, and temperature. This is important for enhancing the effectiveness of drugs and minimizing their side effects. The present utilization of MOFs is restricted to a few classifications, including ZIF, Materials Institute Lavoisier (MIL), and University of Oslo (UIO). Moreover, recent instances documented in the literature have shown the potential of MOFs for biomedical uses. The use of core-shell MOFs in treatment systems has been widely researched. Instead of relying solely on traditional methods like chemotherapy (CT), photothermal therapy (PTT), photodynamic therapy (PDT), or immunotherapy, core-shell MOFs can serve as carriers for therapeutic agents and as active treatment components. Even more exciting is the potential for imaging-guided multimodal therapies, where chemo/PTT, chemo/PDT, and many others work synergistically to combat tumors more effectively. To achieve this, we can modify the structure of core-shell MOFs or load them with targeted molecules and imaging agents, making the fight against cancer even more precise. The future of cancer treatment is bright, and core-shell MOFs could play a pivotal role. Ultimately, we will investigate the potential opportunities and obstacles to using MOFs in biomedical applications. Compared to other extensive evaluations concerning the uses of MOFs in biomedicine,<sup>21,23</sup> this feature article will focus on specific research on core-shell MOFs in the four areas mentioned above in recent years, offering researchers a thorough grasp of the present state and exciting advancements of MOFs in this area from diverse viewpoints.

## 2. Preparation strategies of core-shell MOFs

### 2.1. Preparation strategies of core@MOF and MOF@shell

The placement position of the MOF in the core-shell arrangement may be different.<sup>21</sup> The MOF serves as a protective layer for the core, ensuring it remains intact and preventing the core from leaching and accumulating independently during the entire reaction process. It creates a stable and continuous environment that is highly conducive to the reaction. In addition, when MOFs are employed as the outer materials, producing a consistent single crystal or polycrystalline MOF layer becomes feasible by controlling the circumstances. The attainment of uniformity requires other usual arrangements of MOF composites. The core@MOF structure is classified based on various core compositions: metal nanoparticles@MOF, metal oxides@MOF, metal sulfides@MOF, and, other nanoparticles@MOF. The composites at the core of MOFs are formed by uniformly coating the outer layer of another material with the MOF shell through a combination of physical and chemical techniques. This procedure entails carefully coating the MOF shell to guarantee consistency and durability. The materials comprising metal nanoparticles@metal-organic frameworks with core-shell configurations exhibit customizable shapes and evenly dispersed nanoparticles. These materials have garnered significant attention in biomedicine



because of their exceptional physical and chemical properties, versatility, stability, and dispersibility. The metal nanoparticle core is effectively encapsulated within a MOF shell, serving as a robust substrate for the nanoparticles. The core-shell structure of metal sulfide@MOF has been the subject of extensive attention up to this point. Most metal sulfides have a relatively small bandgap, which is a notable advantage compared to most metal oxides. Semiconductor materials composed of sulfide@MOF are widely utilized in biology and medicine to serve as targeted attachments for various entities, including proteins, cells, acidic components of the nucleus, viruses, and so on. Metal oxides with semiconductor properties, such as  $\text{TiO}_2$ ,  $\text{ZnO}$ , and  $\text{Fe}_3\text{O}_4$ , have been extensively researched and proven valuable in the field of biomedicine. Integrating MOFs with metal oxides can greatly enhance biomedical efficacy. The synthesis of these structures is of particular importance due to their applications in biomedicine, and there are a wide range of synthetic methods to achieve these structures, which include one-pot approaches, *in situ* growing methods, self-template methods and layer-by-layer assembly (LBL) assembly, (Fig. 1) and each of these methods have their unique feature according to the structure of core@MOF (Table 1).<sup>21,24,25</sup>

By integrating MOFs as the core element and effectively layering them with complementary materials, we can fully harness the MOF core's and outer shell's exceptional biomedical properties. This innovative approach enhances functionality and opens up new avenues for advanced composite materials in biomedical applications. Employing MOFs as the primary materials because of their exceptional elasticity facilitates a robust chemical connection between the MOF core and the shell, allowing for integrating specific functions that enhance shell assembly. Furthermore, using a sturdier porous material for the outer layer can protect the relatively unstable MOF without blocking its pores, thus maintaining its significant surface area and porous structure, crucial for enhancing biomedical applications. The MOF@shell structure can be mainly classified as MOF@metal sulfides, MOF@COF, and MOF@other materials.<sup>24</sup> Researchers have shown significant interest in combining MOFs with metal sulfides. It is feasible to minimize the leaching and aggregation of MOF cores due to their instability by creating core-shell structures. In the scenario involving MOF@COF, the covalent organic framework (COF) is a porous crystalline polymer. COFs are composed of light elements interconnected through robust covalent bonds using reticular chemistry. They possess significant

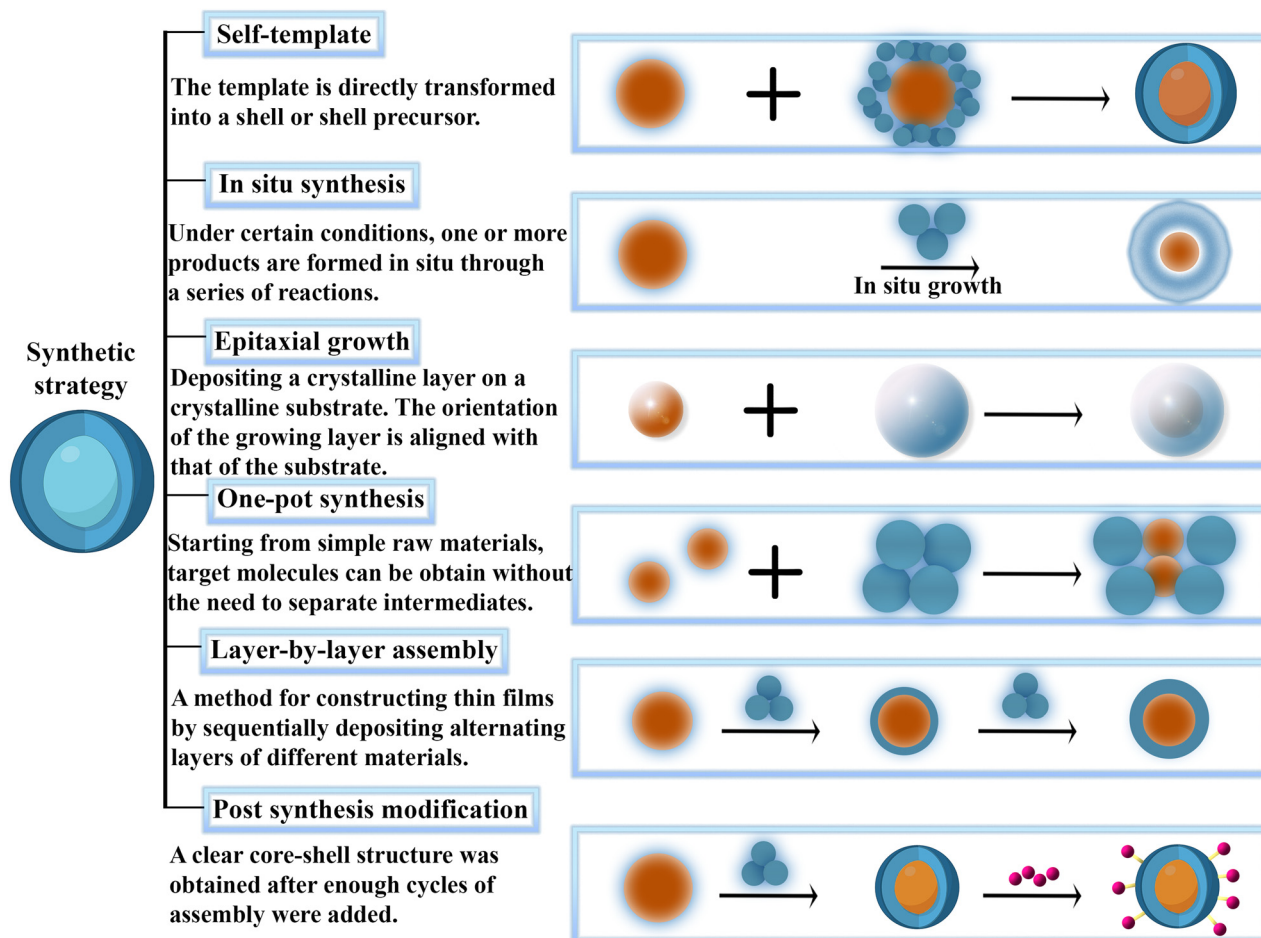


Fig. 1 Schematic diagram of different preparation strategies for MOF core-shells.



Table 1 Summary of data on the preparation of core-shell MOFs

Structure	Composition	Growth mechanism	Ref.
Core@MOF	(Co-MOF)@CoNiO <sub>2</sub>	<i>In situ</i>	26
Core@MOF	(Ti/Ce)UiO-X MOFs@TiO <sub>2</sub>	<i>In situ</i>	27
Core@MOF	CeO <sub>2</sub> @ZIF-8	<i>In situ</i>	28
Core@MOF	Co/MnOx@quasi-MOF-74	<i>In situ</i>	29
Core@MOF	Fe <sub>3</sub> O <sub>4</sub> @MIL-100(Fe)	<i>In situ</i>	30
Core@MOF	Fe <sub>3</sub> O <sub>4</sub> @MIL-101-SO <sub>3</sub>	<i>In situ</i>	31
Core@MOF	MOF-Ti@PANI	<i>In situ</i>	32
Core@MOF	Pd@ZIF-8	<i>In situ</i>	33
Core@MOF	Pt/CeO <sub>2</sub> @UIO-66-NH <sub>2</sub>	<i>In situ</i>	34
Core@MOF	RhB@ZIF-71	<i>In situ</i>	35
Core@MOF	Ti <sub>x</sub> Fe <sub>1-x</sub> O <sub>y</sub> @Fe <sub>2</sub> O <sub>3</sub>	<i>In situ</i>	36
Core@MOF	Z67@CNF	<i>In situ</i>	37
Core@MOF	Au@MOF-5	One-pot	38
Core@MOF	Au@MOF-74	One-pot	39
Core@MOF	CdS@ZIF-8	One-pot	40
Core@MOF	Fe <sub>3</sub> O <sub>4</sub> /CNC@ZIF-8	One-pot	41
Core@MOF	Pt@ZIF-8	One-pot	42
Core@MOF	Ru@HKUST-1	One-pot	43
Core@MOF	SiO <sub>2</sub> @50Benz-Cys	One-pot	44
Core@MOF	TGZ@eM	One-pot	45
MOF@Shell	Co-SA/P	<i>In situ</i>	46
MOF@Shell	HKUST-1@Ag	<i>In situ</i>	47
MOF@Shell	ZrMOF@MnO <sub>2</sub>	<i>In situ</i>	48
MOF@Shell	CoS <sub>2</sub> /WS <sub>2</sub>	One-pot	49
MOF@Shell	DNAzyme@Cu/ZIF-8	One-pot	50
MOF@Shell	DPGG@UiO-66	One-pot	51
MOF@Shell	PCN-222@Zr-BPDC	One-pot	52
MOF@Shell	pt@ZIF-8	One-pot	53
MOF@Shell	ZIF-67@SiO <sub>2</sub>	One-pot	54
MOF@Shell	MOF-235@PEG@silica	Self-template	55
MOF@MOF	MIL-88B@MIL-88A	Epitaxial growth	56
MOF@MOF	Co-MOF-74@Mn-MOF-74	Epitaxial growth	57
MOF@MOF	Cu-MOF@Co-MOF	Epitaxial growth	58
MOF@MOF	Fe-MIL-88B@Fe-MIL-88C	Epitaxial growth	59
MOF@MOF	IRMOF-2@MOF-5 Janus particles	Epitaxial growth	60
MOF@MOF	MnFe-X PBAs	Epitaxial growth	61
MOF@MOF	NH <sub>2</sub> -MIL-88B(Fe)@ZIF-8	Epitaxial growth	62
MOF@MOF	Ni-MOF-74@Co-MOF-74	Epitaxial growth	63
MOF@MOF	UiO-66-(OH) <sub>2</sub> @UiO-66-NH <sub>2</sub>	Epitaxial growth	64
MOF@MOF	UiO-66@67-bpy	Epitaxial growth	65
MOF@MOF	UiO-66@UiO-67	Epitaxial growth	66
MOF@MOF	UiO-66-NH <sub>2</sub> @Ni-MOF	Epitaxial growth	67
MOF@MOF	UiO-67@Ni-MOF	Epitaxial growth	68
MOF@MOF	UiO67@Rh@UiO66	Epitaxial growth	69
MOF@MOF	ZIF-67@Co-MOF-74	Epitaxial growth	70
MOF@MOF	ZIF-67@ZIF-8	Epitaxial growth	71
MOF@MOF	ZIF-L@ZIF-67	Epitaxial growth	72
MOF@MOF	Zn-MOF@Co-MOF	Epitaxial growth	73
MOF@MOF	NH <sub>2</sub> -MIL-101(Al)@ZIF-8	Epitaxial growth	74
MOF@MOF	ZIF-L(Co)@ZIF-8	Heteroepitaxial	75
MOF@MOF	PMOF-3@HHU-9	One pot	76
MOF@MOF	NJU-Bai21@HHU-9	One pot	76
MOF@MOF	PMOF-3@NJUBai21	One pot	76
MOF@MOF	ZIF-11@ZIF-8	Post-modifications	77

potential across a wide range of applications. The advantages of core-shell MOFs@COFs are as follows: (1) the adjustable properties of MOFs and COFs make it highly efficient to establish strong reinforcement interactions between the MOF cores and COF shells, ensuring sufficient protection for the COF layer to avoid detachment. (2) COFs have a higher photoconductivity and charge mobility than MOFs with low conductivity because they can adequately store the p arrays. There are significantly fewer records of composites with MOFs as the central components compared to those that feature MOFs as the outer layer. This may be attributed to the challenge of reactants penetrating the shell for further

reactions when the MOF is utilized as the core. The issues can be tackled by considering the following factors: (1) utilizing a highly absorbent outer layer allows reactants to flow through its pores effortlessly, facilitating a seamless one-step reaction process. (2) Tweaking the thickness of the shell layer can boost the movement and mixing of reactants, leading to a significant increase in electron transfer efficiency. (3) The core and shell synergize, forming a strong covalent bond. The MOF core creates a contained setting for the reaction system. Simultaneously, the shell, which has a customizable pore size, can selectively permit beneficial substances to enter while preventing the escape of active components, enhancing their effectiveness, or allowing for a specific degree of separation. The creation of these formations is significant because of their use in biomedicine. Various synthetic methods produce these formations, such as the one-pot, *in situ* growing, and self-template methods (Fig. 1),<sup>21,24,78</sup> and these methods are similar to the synthesis of core@MOF structures. All these methods are compared and reviewed in Table 2.

**2.1.1. *In situ* synthesis.** Using *in situ* synthesis involves growing one or more guests within a substrate (host) under specific conditions. When this method is used, the composites prepared have guest components nucleated in the metal matrix, which results in spontaneous growth. Consequently, the molecules of the matrix and guest demonstrate excellent compatibility and form strong interfacial bonds. This method is advantageous for creating highly stable core@MOF and MOF@shell structures.<sup>24</sup> The *in situ* growth method requires less preparation than the surface modification method because it doesn't require an extra modification step<sup>21</sup> and the concentration of reactants can be adjusted to control the size and morphology of composites, providing a new method for producing distinctive core-shell structures.<sup>24</sup> Li *et al.* provided a detailed method for growing the Fe-MOF in place on CuS nanoplates. The procedure started by creating CuS nanoplates using the hydrothermal technique. These nanoplates were later mixed into an ethanol solution with FeCl<sub>3</sub>. After adding H<sub>3</sub>BDC, the mixture was agitated, which effectively initiated the *in situ* growth of Fe-MOF shells on the single-core CuS. The precise methods of SEM were used to observe the composite core-shell structure for CuS, while TEM was used for the composite. This careful observation process ensures the accuracy and reliability of the research findings.<sup>24</sup> Meng *et al.* utilized *in situ* encapsulation technology for the production of core-shell Pt@UiO-66-NH<sub>2</sub> composites. The interplay between environmental factors created a protective buffer layer that enhanced the relationship between the nanoparticles and the porous structure. To modify the pre-synthesized Pt nanoparticles, a surfactant was needed to mix the dispersed nanoparticles into the MOF precursor solution for the next stage of our reaction. The enhanced composites created layered voids by leveraging the instability of the MOF in the presence of Pt NPs in this approach. The SEM and TEM images showed that the stacked empty spaces were evenly spread out around the nanoparticles and helped preserve the MOF shell's structure.<sup>85</sup> Wang *et al.* created core-shell composites by utilizing MIL-125@In<sub>2</sub>S<sub>3</sub>. They conducted a solvothermal process by mixing In(NO<sub>3</sub>)<sub>3</sub>, 3xH<sub>2</sub>-O, and CS<sub>2</sub> with



Table 2 Comparison of the preparation methods for MOFs

Preparation method	Key characteristics	Advantages	Disadvantages	Examples/notes	Ref.
Self-template method	The MOF core acts as both a template and a precursor and transforms into the shell	Efficient use of material and no need for external template	Restricted to convertible MOFs and necessitates exact conditions	ZnO@ZIF-8	79
One-pot synthesis	Core and shell precursors added simultaneously; self-assembly leads to core-shell formation	Time-saving; fewer steps	Less control over distinct core/shell structures	UiO-66@SiO <sub>2</sub> /less common for precise architectures	80
Layer-by-layer (LbL)	Precursors are introduced in stages, with washing conducted in between to create accurate layers of the shell	High control over shell thickness and composition	Time-consuming; labor-intensive	Fe <sub>3</sub> O <sub>4</sub> @UiO-66-NH <sub>2</sub> /often used in thin films or surface coatings	81
Epitaxial growth	Shell grows directly on the core with lattice match	Produces seamless, highly ordered interfaces	Requires strict lattice match; fewer material combinations	UiO-66@ZIF-8/often seen in isorecticular MOFs	82
Post-synthetic method	Shell material deposited onto core MOF post-synthesis	Flexibility in material choice; works with fragile cores	Might cause partial damage to the core or incomplete coating	ZIF-67@Co-MOF-74/used for hybrid/heterostructures	83
<i>In situ</i> method	The core formed on the template surface and then the shell built around it	Can form hollow/complex structures	Requires template removal if undesired	Pt@UiO-66-NH <sub>2</sub> /useful in hierarchical or porous structures	84

the MIL-125 solution. This process formed In<sub>2</sub>S<sub>3</sub> nanosheets on the MIL-125 core, forming a stable and protective shell. The Ti-MOF's substantial surface area and plentiful pore structure made it well-suited for coating with In<sub>2</sub>S<sub>3</sub>. The results were validated using SEM and TEM images.<sup>84</sup> Ding *et al.* conducted a study in which they developed a core-shell composite material of Fe-MOF-74@SiO<sub>2</sub> by synthesizing a SiO<sub>2</sub> layer on Fe-MOF-74 *in situ*. The application of the SiO<sub>2</sub> coating significantly enhanced the interaction between Fe ions and the organic linking groups in Fe-MOF-74, creating a more dynamic and effective composite with better water stability. The application of the SiO<sub>2</sub> layer was confirmed using SEM, and the findings were validated through FT-IR and TG analyses.<sup>86</sup>

**2.1.2. One-pot synthesis.** One-pot synthesis is a standard and easy-to-use synthesis method that can work with primary and readily available raw materials and instantly create intricate molecules with complex structures without having to separate intermediates. This approach has the potential to greatly reduce the overall number of reaction steps involved in the process, leading to energy savings, simplifying production and post-treatment on a large scale, and improving reaction efficiency.<sup>78</sup> One-pot synthesis involves simultaneously introducing metal oxygen clusters and organic ligands into a particular system, followed by auxiliary synthesis. One-pot synthesis eliminates expensive processes, shortens reaction times, and saves money. At the same time, the purification and impurity removal steps are naturally skipped because there isn't a complex multistep reaction.<sup>11</sup> One-pot synthesis is suitable for specific cases, for instance, when: (1) the precursor chemicals are unstable, toxic, or hazardous. (2) It is advantageous to have intermediate reactants in order to produce the final products. (3) Chemical balance has been achieved between the initial materials and intermediary reactants.<sup>78</sup> Bao *et al.* created a core-shell nanoparticle by employing Fe-MIL-100 as the shell and UCNPs as the core through a self-assembly process that occurred in one step. The Fe-MIL-100 MOF shell is a MOF formed by coordinating Fe<sup>3+</sup> ions with the carboxyl groups of BTC ligands. This shell plays an

essential role in the properties of the nanoparticle, such as its stability and reactivity. The UCNPs were simultaneously encapsulated in the shell, while the pores of Fe-MIL-100 were filled with the photoacid generator (PHP). The nano-agent, measuring around 130 nm in size, showed the typical core-shell architecture in the TEM images.<sup>87</sup> Meng *et al.* utilized a nanocarrier based on a MOF, in which the coordinating metal was zinc (Zn<sup>2+</sup>) and the organic ligand consisted of a disulfide-containing imidazole. They also generated a control MOF nanocarrier using an imidazole ligand that did not contain disulfide. Both varieties of nanocarriers were equipped with a model photosensitizer (chlorine e6/Ce6). The researchers effectively produced this structure using the one-pot method. Examination and imaging demonstrate the creation of the core-shell structure. However, ligands that contain disulfide bonds are sophisticated and can facilitate more effective drug delivery, but the issue of ligand instability while in circulation needs to be resolved.<sup>88</sup> Zhang *et al.* accomplished an impressive achievement in synthesizing core-shell UiO-66@SiO<sub>2</sub> microspheres. They began the development of the Zr-MOF on the outer surface of SiO<sub>2</sub> microspheres, where SiO<sub>2</sub> acts as the core and the MOF functions as the outer layer. The combination of ZrCl<sub>4</sub>, DMF, H<sub>2</sub>BDC, and amino SiO<sub>2</sub> in a round-bottom flask for solvothermal synthesis is noteworthy. They demonstrated a remarkable ability to precisely control the thickness and density of the MOF shell by adjusting the concentration of the Zr<sup>4+</sup> precursor, as well as the reaction duration and temperature. This marks a significant breakthrough in the field of materials science and utilizing this method with other MOFs and multi-layered structures may improve their application in theranostics. This study establishes the foundation for adaptable and scalable MOF coatings.<sup>80</sup>

**2.1.3. Self-template method.** In recent years, there has been significant research on using templates to create structured materials, particularly in relation to MOFs. The methods for using templates to manipulate structure are evolving. The exploration of MOFs has taken an exciting turn as researchers delve into the intricacies of modifying metal linkages and



bonding characteristics. The traditional method effectively employs templates and emphasizes the strategic modification of surfaces with specific functional groups, thereby significantly influencing the growth of MOFs on substrate templates. However, a major obstacle is the difficulty in preventing the autonomous nucleation and growth of MOFs in solution. The self-template strategy has been suggested as a way to tackle this problem, providing a solution that instills confidence in managing the nucleation and growth of MOFs. This method creates MOFs with specific and consistent shapes by utilizing a template that not only provides support for the outer layer but also converts into the outer layer or its precursor, playing a role in forming the outer layer. In this context, metal oxides have been effectively utilized as preliminary templates to control the nucleation site, enabling precisely defined core-shell structures to form through the loss of their metal ions. Furthermore, employing the self-template method allows the creation of core-shell nanomaterials to particular sizes and structures by modifying the amount of solvent used and the duration of the reaction. In this method, the template provides a supportive foundation and releases metal sources to aid in shell formation. The creation of core-shell structures is made more accessible by having consistent metal ions in the MOF's core and shell parts, simplifying the synthesis procedure. The self-template approach is straightforward and user-friendly, yet the selection of materials is restricted due to the requirement for the core and shell's metal compositions to align.<sup>24</sup> Zhang *et al.* created a core-shell structure featuring pores made of copper hydroxy sulfate@MOF, which is enhanced with 2,5-dimercapto-1,3,4-thiadiazol (DMTZ) through a straightforward self-template technique to capture Hg<sup>2+</sup>. Encasing the copper hydroxy sulfate (CHS) core with a MOF shell was essential to inhibit the self-nucleation of MOFs (Cu<sub>3</sub>(BTC)<sub>2</sub>) in the solution and to streamline the intricate multistep processes. The CHS metal source experienced an *in situ* change, forming a distinct Cu<sub>3</sub>(BTC)<sub>2</sub> crystal. The DMTZ-modified CHS@Cu<sub>3</sub>(BTC)<sub>2</sub> (CHS@Cu<sub>3</sub>(BTC)<sub>2</sub>-DMTZ) was analyzed using X-ray diffraction (XRD), SEM, and nitrogen sorption-desorption isotherms (BET) to evaluate its composition and characteristics. Enhancing DMTZ functionalization enables the detection of various toxic metal ions, thus expanding the method for environmental cleanup. The *in situ* conversion of the CHS template into an active MOF while maintaining a core-shell architecture showcases an innovative and effective synthesis approach with practical applications in the real world.<sup>89</sup> Zhan *et al.* successfully developed a core-shell heterojunction featuring ZnO@ZIF-8. In a synthesis process, ZnO nanorods intertwined with organic ligands were mixed with a blend of DMF and water, which released Zn<sup>2+</sup> ions into the solution. This dynamic interaction resulted in the formation of a ZIF-8 shell that enveloped the nanorods. The ZnO nanorods acted as a sacrificial template and a source of zinc, while 2-methylimidazole served as both an organic ligand and an etching agent. As the reaction progressed, the surface of the ZnO nanorods developed a textured appearance, and a delicate layer of ZIF-8 crystals gradually formed around them. Over time, the thickness of the ZIF-8 shell increased, ultimately creating a seamless and

protective coating that beautifully encapsulated the nanorods. The self-template approach, showing impressive adaptability, revealed its capability by concurrently generating ZnO@ZIF-8 nanorods and nanotube structures. This novel approach is used to develop core-shell structures of MOFs straightforwardly and effectively, inspiring new avenues for your research. This approach effectively integrates template removal with shell creation in one step, providing a framework for scalable and innovative material production. It ensures consistent shell thickness throughout the gradual etching process while preserving the nanorod structure as the template is consumed.<sup>79</sup> Lin *et al.* reported that ZIF-67 was a template for creating ZIF-67@CoLDH/SiO<sub>2</sub> nanomaterials with a core-shell/yolk-shell/hollow structure. The reaction time was adjusted to accomplish this. CTAB was included as a protective agent to reduce the etching rate of the MOF. They used CTAB to gradually remove ZIF-67 to release Co<sup>2+</sup> ions as metal suppliers, forming Co-LDH shells. The creation of core-shell materials using MOFs as the core layer had yet to be documented before this work. Therefore, modifying the protective agent and reaction time represented a new method for preparing MOF@shell structures. This research presents an innovative aspect of MOF-based design by facilitating the regulation of shell development and structural changes over time and through surfactant adjustments, managing the etching speed to prevent the collapse of the MOF core, and precisely adjusting the morphology of hybrid shell structures.<sup>90</sup>

**2.1.4. LBL assembly.** LBL assembly is a method for applying materials onto a substrate one layer at a time. The process begins by having a charged material adhered to a substrate with an opposite charge, which cancels out the surface charge. The substrate is coated with alternating layers of materials carrying opposite charges until the desired number of layers is achieved. The LBL assembly, known for its simplicity, was mainly employed on flat substrates due to its straightforward synthesis process, involving submerging the substrate in a polymer solution and washing away any uncoated material. Lately, a growing focus has been on using LBL assembly to create core-shell materials. The technique has been extensively used to develop MOF materials by gradually depositing metal ions and organic linkers onto the central matrix. It is essential to alter the matrix surface to aid in the growth of MOFs. The effectiveness of the LBL assembly is influenced by the number of deposition layers and specific assembly conditions. This can modify the properties of the resulting composites, including their thickness, function, and composition. By meticulously adjusting the number of assembly cycles, a specific core-shell structure can be achieved, enabling precise control over the growth of MOFs.<sup>24</sup> Ehrling *et al.* utilized the LBL assembly technique to apply coatings of two different types of MOFs (MIL-101-NH<sub>2</sub> and UiO-67) onto SiO<sub>2</sub> microspheres, resulting in the formation of core-shell structures SiO<sub>2</sub>@MOF and SiO<sub>2</sub>@MIL-101-NH<sub>2</sub>, respectively. They explored the impact of the LBL assembly process on the thickness of the MOF shell. After 20 assembly cycles, they successfully developed a core-shell structure coated with MIL-101-NH<sub>2</sub>, and the MOF's reflection was observed after just 15 cycles of UiO-67. Enhancing the number



of cycles could create a uniform layer and a core-shell configuration. The MOF was built up layer by layer and then utilized as a coating on silicon spheres for its application as an HPLC stationary phase. This combination of silicon balls provides remarkable packing characteristics and MOFs' superior separation capabilities.<sup>91</sup> Chen *et al.* created the Fe<sub>3</sub>O<sub>4</sub>@UiO-66-NH<sub>2</sub> composite by utilizing a LBL epitaxial growth technique. They achieved their goal by strategically immersing Fe<sub>3</sub>O<sub>4</sub> nanoparticles in a series of ethanol solutions, each infused with a metal node precursor [Zr<sub>6</sub>O<sub>4</sub>(OH)<sub>4</sub>]<sup>12+</sup> and organic linkers like NH<sub>2</sub>-BDC (2-amino terephthalic acid). To top it off, they skillfully separated the mixture using a magnet, showcasing a fascinating blend of chemistry and finesse. The meticulous process led to the validation of the analysis findings, which confirmed that composites of Fe<sub>3</sub>O<sub>4</sub>@UiO-66-NH<sub>2</sub> with a Zr6 node content of 24.4 μmol g<sup>-1</sup> exhibited a clear core-shell structure and excellent thermal and chemical stability.<sup>81</sup>

## 2.2. Preparation strategies of MOF@MOF

The initial preparation of core-shell structured MOF@MOF single crystals through epitaxial growth was first proposed by Kitagawa *et al.* in 2009.<sup>92</sup> This marked the beginning of the narrative surrounding these types of porous coordination polymer (PCP) materials. The formation of MOF@MOF hybrid materials involves the addition of different organic ligands after crystal nucleation, allowing for combining two or more distinct types of MOFs into a single unified hybrid material comprising MOF-on-MOF. Usually, these hybrid structures are composed of two types of architectures: a MOF can be completely enclosed by another MOF, resulting in a core-shell structure known as MOF@MOF. Additionally, a MOF can be strategically grown on the surface of another MOF in either an isotropic or anisotropic manner, leading to a layered MOF-on-MOF configuration.<sup>93</sup> The focus here is on core-shell structures, as these materials offer enhanced performance across a wider range due to increased structural diversity and more opportunities for improving surface properties, sometimes resulting in the emergence of new features.<sup>94</sup> To successfully develop MOF@MOF hybrids, aligning the lattice of the second metal building unit with that of the initial MOF core is essential. For instance, MOFs from the MIL, ZIF and UiO-66 and various other MOF structures are commonly used as the foundation and integrated into an additional MOF layer. The MOF@MOF framework boasts a range of significant advantages, such as its flexible structures, extensive surface area, and high porosity. It features abundant exposed active sites and demonstrates excellent biocompatibility and remarkable biological activity. Its robust chemical and colloidal stability ensures reliability, while efficient surface modification enhances its functionality. Furthermore, functional groups like -NH<sub>2</sub> and -COOH in MOFs contribute to their impressive capabilities. They have been utilized as practical bases that enhance the ability to immobilize antibiotics and biomolecules, including glucose, antibodies, and aptamers.<sup>93</sup> The methods for creating these structures will now be examined, which include epitaxial growth, post-synthetic modification, and one-pot synthesis (Fig. 1).<sup>95</sup>

**2.2.1. Epitaxial growth.** Epitaxial growth opens up exciting possibilities for creating hybrid MOF@MOF structures with tailored compositions and intricate architectures. This fascinating process involves layers of crystalline materials carefully applied to a selected face of a substrate crystal. This intricate process requires precise alignment and both materials must share the same orientation and have comparable lattice spacings. By using epitaxial growth, researchers can effectively synthesize MOF@MOF hybrids. When two MOFs have compatible cell lattices, the development of a secondary MOF on a pre-existing one becomes much easier. However, if there are significant differences in their lattice parameters, the growth can be hindered, often leading to the independent formation of the second MOF instead. This method really shines when it comes to creating complex hierarchically structured MOF@MOF heterostructures.<sup>82</sup> The first step is establishing a host MOF with well-defined surfaces to act as a substrate. Next, a guest MOF that matches the host MOF's facet orientation and lattice spacing is deposited epitaxially at the interface.<sup>96</sup> MOF@MOF hybrids that possess the same ligand length and topological configuration can be readily combined, with a second MOF layer developed over the surface of the MOF core using the internally extended growth technique.<sup>93</sup> Generally, the effective development of a secondary MOF on an already established MOF is due to their compatible cell lattices, which have low interface energy.<sup>82</sup> Core-shell hybrid structures comprising two different MOFs featuring diverse ligands and morphological characteristics have been created. Because of their elevated surface energy, characteristics can be challenging in achieving consistent epitaxial growth. MOF@MOF heterostructures of this kind are typically created through a surfactant-assisted overgrowth process. Surfactants such as CTAB and PVP are fascinating in shaping MOF@MOF heterostructures. By reducing surface energy, they pave the way for innovative developments in these complex structures, unlocking their application and performance possibilities.<sup>93</sup> Zhan *et al.* conducted a study on ZIFs, which are a class of MOFs made up of transition metal cations (primarily Zn or Co) that are connected by ligands derived from imidazole. ZIFs have a structure similar to zeolites and exhibit significant porosity and thermal solid and chemical stability. Among the ZIFs, ZIF-8 and ZIF-67 are two that are frequently encountered. Both are built using the organic linker 2-methylimidazole (HMeIm) and display comparable crystallographic characteristics. Nonetheless, they feature distinct metal centers, with Zn present in ZIF-8 and Co utilized in ZIF-67. Due to their identical lattice constants, ZIF-8 and ZIF-67 can undergo various forms of heteroepitaxial growth. The development of a ZIF-8@ZIF-67 heterostructure starts with the synthesis of ZIF-8 seeds. The seeds are subsequently utilized to attach Co<sup>2+</sup> ions to their surface by means of coordination interactions with the available HMeIm. A ZIF-67 shell is created around the ZIF-8 through coordination with extra HMeIm linkers. A ZIF-67 shell is created around the ZIF-8 through coordination with extra HMeIm linkers. The presence of ZIF-L particles enables the formation of a well-structured leaf-shaped core-shell ZIF-L@ZIF-67 by blending Co<sup>2+</sup> and HMeIm at approximately room temperature. The number of ZIF-67 shell components is dictated by the quantities of Co<sup>2+</sup> and HMeIm employed. Developing one



MOF layer over another existing MOF can create a MOF@MOF heterostructure with a distinct shape. This study demonstrates how lattice-matched MOFs can facilitate controlled assembly of MOFs on top of one another. This approach achieves high crystallinity, structural compatibility, and diverse morphologies, making it suitable for advanced functional applications. They explore multi-shell architectures using different ZIFs or by doping with metals. This allows for customizing properties such as permeability or selectivity for gas separation or drug delivery.<sup>96</sup> Tsung *et al.* synthesized heterostructures comprising UiO-66 encapsulated in ZIF-8. ZIF-8 and UiO-66 possess distinct chemical compositions and structures. ZIF-8 crystals consist of zinc clusters and imidazolate, while UiO-66 comprises zirconium clusters coordinated with hydroxide and carboxylate linkers. The key to their synthesis was the use of CTAB, which allowed them to create consistent ZIF-8 outer layers on uniformly distributed UiO-66 crystals, leading to the synthesis of the UiO-66@ZIF-8 hybrid. Employing surfactants and polymeric stabilizers to generate a broader range of chemically diverse MOF combinations facilitates the creation of hybrid systems with customized physicochemical characteristics. The approach that utilizes surfactants effectively resolves structural discrepancies, indicating potential new design principles for MOF hybrid interfaces.<sup>82,93</sup>

**2.2.2. One-pot synthesis.** In the past, the creation of MOF@MOF required a sequential speed-mediated growth process. This involved preparing the core MOF crystal and using it as a seed to grow the shell MOF. The intricate synthetic procedures and the principle of lattice matching, which often led to limitations in the process, restricted the advancement of this technique. There has been a growing emphasis on a single-step synthesis of MOFs@MOFs; in this approach, the metal ions and ligands are released from the inner and outer MOFs into the reaction system at the same time, creating a dynamic interplay that enhances the overall reaction efficiency. This approach offers a solution to these limitations.<sup>94</sup> The one-pot synthesis process includes combining the precursors in a solvent and allowing them to react while stirring. Advantages of this approach include affordability, high production capacity, and easily attainable experimental parameters. Furthermore, it's a very manageable procedure because researchers can introduce reactants at any reaction stage. The one-pot method typically synthesizes MOFs with impurities, rendering them unsuitable for applications that demand high purity.<sup>97</sup> A typical and easy method is a one-pot synthesis, which uses readily available raw materials to produce complex molecules with intricate structures without separating intermediates. This method reduces the number of reaction steps, conserving energy and enhancing reaction efficiency. The one-pot growth technique successfully envelops from the outer layer to the inner core, leading to a well-defined core-shell structure with a uniform size distribution.<sup>98</sup> Zou *et al.* demonstrated the simultaneous creation of heterometallic ZIF-67@ZIF-8 using Zn and Co ions as connection points and 2-methylimidazole as the organic binder. This was attributed to the distinct nucleation kinetics of Zn and Co ions. The preparation of ZIF-8 occurred in a standard two-step process, with initial weak scattering seen in

the first step (after approximately 1 minute), indicating the rapid formation of the nucleus, followed by a continuously rising kinetic curve in the second step as the ZIF-8 nucleus grew. The scattering signal for ZIF-67 showed a sudden increase starting from 1 minute, and the reaction finished within 2 minutes, demonstrating faster one-step growth kinetics. Consequently, a range of Co/Zn ZIFs ( $\text{Co}_x\text{Zn}_{100-x}\text{-ZIF}$ , where  $x$  represents the molar percentage of Co) were created by combining two metals and the identical 2-methylimidazole ligand in one pot.<sup>93,99</sup> Zhou *et al.* developed a core-shell structure of PCN-222@ZrBPDC using a one-step synthesis method. The lattices of both PCN-222 and Zr-BPDC were not aligned. The  $\text{Zr}^{4+}$  is firmly attached to TCPP on PCN-222, resulting in the rapid and even formation of crystals. Under similar experimental conditions, crystal formation occurred more slowly with BPDC (BPDC  $\frac{1}{4}$  biphenyl-4,40-dicarboxylate) than with TCPP. Using the seed crystal as the foundation for the second MOF resulted in accelerated heterogeneous nucleation in contrast to its homogeneous equivalent. The core-shell PCN-222@Zr-BPDC hybrid was created by combining  $\text{Zr}^{4+}$  ions with H4TCPP and H2BPDC.3, resulting in the production of the hybrid.<sup>88,96</sup> Finally, the creation of the core-shell structured MOF was significantly simplified, as there was no need for an additional functionalization step, thanks to the one-pot method. The work above showed that this approach demands specific reaction conditions and controls the shell layer's growth by modifying the concentration of reactants, reaction duration, and temperature. This undeniably raises the complexity of the synthesis. Nevertheless, this approach has proven certain benefits, including the ready accessibility of initial materials, a small number of reaction stages, and the capacity to utilize starting components in complete alignment with the economic principle. This approach allows for the orderly and uniform introduction of guest molecules into MOFs while quickly synthesizing complex core-shell structures. It is characterized by its simplicity and cost-effectiveness, making it well-suited for industrial production and deserving of further investigation.<sup>98</sup>

**2.2.3. Post-synthetic modification.** The inner porosity of MOFs can be functionalized using post-synthetic modification (PSM) techniques, first developed by Lobkosky *et al.* in 1999 and then by Kim *et al.* in 2007. The term "post-synthetic modification" was coined by Cohen and Wang in 2007, leading to further progress in the field. Similar PSM methods can also modify only the outer surface of crystals.<sup>100</sup> A method for modifying post-synthetic processes allows for the versatile creation of core-shell MOFs@MOFs. This part presents the strategies for modifying post-synthetic processes, which include the methods of selective transmetalation, exchanging ligands after synthesis, the internal extended growth method, the surfactant-mediated overgrowth method, and the retrosynthetic design.<sup>94</sup>

**2.2.3.1. Selective transmetalation method.** The selective transmetalation method is an alternative approach to creating MOF@MOF composites through post-synthetic modification. One of the strategies for post-synthetic modification involves



replacing the structural metal ions that are part of the MOF connectivity. Lah *et al.* researched four isostructural MOFs that exhibit different levels of stability, specifically  $M_6(\text{BTB})_4(\text{BP})_3$  (referred to as ITHD crystals) where M represents Zn(II) (1), Co(II) (2), Cu(II) (3), and Ni(II) (4), BTB represents 1,3,5-benzenetribenzoate, and BP represents 4,4'-dipyridyl. The development of core-shell heterostructures *via* epitaxial growth involves a core crystal that is thermodynamically stable paired with a less stable shell crystal, which is a process of significant importance. The innovative kinetically regulated transmetalation processes we're proposing will revolutionize the creation of core-shell heterostructures, specifically 1@2, 1@3, and 1@4. By immersing the thermodynamically unstable structure 1 in solutions containing Co(II), Cu(II), and Ni(II), we are leading the way in a selective transmetalation technique that will redefine how we synthesize core-shell MOFs@MOFs.<sup>94,101</sup>

**2.2.3.2. Post-synthetic ligand exchange.** Rosi *et al.* were the first to report the creation of MOFs@MOFs with varied structures and directional porosity gradients using post-synthetic ligand exchange, underscoring the critical function of organic ligands in MOF preparation. This research paves the way for potential breakthroughs in the field. Following this, Guo and colleagues showcased the successful creation of core-shell structures of ZIF-67@MOFs (with MOFs being Co-MOF-74, Co-BDC, Co-NH<sub>2</sub>BDC, and CoBTC) through a postsynthetic ligand-exchange technique. The system model included the synthesis of ZIF-67 using  $\text{Co}(\text{NO}_3)_2 \cdot 6\text{H}_2\text{O}$  and 2-methylimidazole (2-MI). ZIF-67@Co-MOF-74 with a core-shell structure was created by exchanging 2-methylimidazole (2-MI) with 2,5-dihydroxyterephthalic acid (DHTP). This exchange occurred because DHTP exhibited a more vital coordinating ability than 2-MI. When ZIF-67 encountered DHTP solutions, DHTP took the place of surface-bound 2-MI to bind with cobalt, resulting in the formation of Co-MOF-74 crystals as the outer layer of ZIF-67@Co-MOF-74. The thickness of the Co-MOF-74 shell can be modified by altering the ZIF-67/DHTP mass ratio. The color of ZIF-67@Co-MOF-74 shifted from purple to purple-gray when the concentration of DHTP was increased, indicating the successful preparation of ZIF-67@Co-MOF-74.<sup>42,50</sup> Matzger *et al.* conducted a meticulous investigation into the creation of hierarchical core-shell MOFs@MOFs through post-synthetic ligand exchange. This rigorous approach was undertaken to gain a comprehensive understanding of the post-synthetic ligand exchange process. The cubic MOF-5 model, which utilized benzene-1,4-dicarboxylate (BDC) and zinc acetate clusters to create large pores, was a key focus of the study. Another significant aspect was the selection of 1,4-dicarboxylic acid benzene-2,3,5,6-tetracarboxylic acid ( $\text{H}_2\text{BDC-d}_4$ ) as the additional ligand. The research involved immersing MOF-5 in a tetrahydrofuran (THF) solution with a 0.01 M concentration of  $\text{H}_2\text{BDC-d}_4$  ( $\text{H}_2\text{BDC-d}_4/\text{BDC} = 1:1$ ) for 18 hours. Raman maps of the sliced crystals revealed the formation of core-shell heterostructures, with BDC-d<sub>4</sub> predominantly located at the outer layer, penetrating to a depth of about 80  $\mu\text{m}$ . Extending the soaking period to 72 hours or increasing the temperature to 45 °C resulted in a more significant depth increase of approximately 160  $\mu\text{m}$ .

The research has significant implications for the field of materials science and chemistry. Using dimethylformamide (DMF) as the exchange solvent, which has smaller diffusion coefficients, produced some intriguing results. Through Raman analysis and PXRD measurements, we discovered significant cracking in the crystals after just three days of incubation in a 0.1 M  $\text{H}_2\text{BDC-d}_4$  solution. These findings not only highlight the impact of the solvent choice but also open new avenues for understanding the behavior of these materials under specific conditions. However, the integrity of MOF-5 was maintained, indicating that crystal exchange was caused by ligand diffusion. UCMC-8, which shares the same metal nodes as MOF-5, underwent a fascinating transformation when linked by  $\text{H}_2\text{BDC}$  and 2,6-naphthalene dicarboxylic acid for ligand exchange. Remarkably, this process led to the preparation of an anticipated core-shell structure following a post-synthetic  $\text{H}_2\text{BDC-d}_4$  ligand exchange in a low-concentration environment (0.005 M). The UiO-66 MOF has shown an impressive ability for post-synthetic ligand exchange, resulting in an intriguing core-shell structure. This process highlights the critical role of ligand diffusion, achieved by substituting 10 mol equivalents of  $\text{H}_2\text{BDC-d}_4$  in water at 85 °C for just one hour. These findings shed light on the complexities of post-synthetic modifications and pave the way for innovative designs in hierarchical core-shell MOFs.<sup>93,102</sup>

**2.2.3.3. Internal extended growth method.** In numerous instances, crafting MOFs@MOFs involves using comparable frameworks, often drawing on the same metal nodes or strikingly similar ligands. However, the challenge lies in blending MOFs with entirely different components, as it requires overcoming the barrier of interface energy. However, Kitagawa *et al.* devised an innovative and versatile internal extended growth technique for creating MOFs@MOFs with distinct crystal structures. They created a hybrid MOF-on-MOF heterostructure  $\text{NH}_2\text{-UiO-66@NH}_2\text{-MIL-125}$  by incorporating  $\text{NH}_2\text{-UiO-66}(\text{Zr})$  into the precursor of  $\text{NH}_2\text{-MIL-125}(\text{Ti})$  with the assistance of the structure-directing agent poly(vinylpyrrolidone) (PVP) while using microwave heating. Furthermore, they effectively built different MOF-on-MOF heterostructures, including  $\text{MIL-101}(\text{Cr})@ \text{NH}_2\text{-MIL-125}(\text{Ti})$  and a combination of  $\text{NH}_2\text{-UiO-66}(\text{Zr})/\text{MOF-76}(\text{Tb})/\text{NH}_2\text{-MIL-125}(\text{Ti})$  using this approach. The suggested internal extended growth method not only shows potential but also promises the adaptable creation of multi-compartment MOFs@MOFs, thereby opening new avenues for research and applications.<sup>94,103</sup>

**2.2.3.4. Surfactant-mediated overgrowth method.** An alternative method for creating MOFs@MOFs with different topologies involved using surfactant-mediated overgrowth. Tsung *et al.* meticulously reported the synthesis of core-shell  $\text{UiO-66@ZIF-8}$  using cetyltrimethylammonium bromide (CTAB) in an aqueous solution. The method involved a careful mixing of UiO-66 core crystals, ZIF-8 precursors, and CTAB. The nucleation of ZIF-8 was promoted by subjecting the reaction system to ultrasonication for 5 minutes, after which it was stirred for 3 hours to produce the core-shell  $\text{UiO-66@ZIF-8}$ . The incorporation of CTAB was



found to be essential, as core-shell UiO-66@ZIF-8 could only be synthesized using it. The quantity of CTAB was also a key factor; insufficient CTAB led to incomplete ZIF-8 coverage, whereas the appropriate amount enabled the coating of ZIF-8 with uniform nucleation and overgrowth. The surfactant type significantly influenced the overgrowth of UiO-66@ZIF-8. The addition of compounds such as tetradecyltrimethylammonium bromide (TTAB), methyl pyridinium bromide (CPB), and sodium dodecyl sulfate (SDS) led to the development of the polycrystalline and fractured ZIF-8 coating as they were not able to accurately regulate nucleation and overgrowth. PVP hindered the synthesis of UiO-66@ZIF-8 due to the requirement for appropriate interaction between PVP and the two MOFs in water. The duration of ultrasonication also had a significant impact on the nucleation of ZIF-8. Without ultrasonication, a fractured ZIF-8 layer formed. An unfinished ZIF-8 shell was noted when the sonication duration exceeded 15 minutes. After being sonicated for one hour, a yolk-shell heterostructure was created. After the above discussions, it was hypothesized that the material's growth mechanism occurred in the following manner: Initially, suitable ZIF-8 nuclei were generated under specific ultrasonic conditions. Subsequently, these nuclei adhered to the surface of UiO-66 in a specific orientation due to the presence of CTAB. The small ZIF-8 nuclei, which were evenly distributed, ultimately expanded into the shell. The unique structures of UiO-66 and ZIF-8 provide additional evidence that the use of surfactants in overgrowth can surpass the challenge of creating MOFs@MOFs with mismatched lattices due to structural similarity.<sup>94,104</sup>

**2.2.3.5. Retrosynthetic design.** MOF@MOF materials have significant potential. Preparing and applying these materials promise significant benefits, but their complexity can be quite daunting. This is mainly due to our limited control over the formation process, which makes this task challenging. Zhou *et al.* proposed using a retrosynthetic design method that considers surface modification and stability to create MOF@MOF architectures carefully. A core substrate of PCN-222(Zr) with high chemical stability was used to perform surface functionalization. The substrate was initially subjected to an excess of benzene-1,4-dicarboxylic acid linker for 24 hours. After that, a Zn(NO<sub>3</sub>)<sub>2</sub> solution was added to the reaction system for a duration of 24 hours to promote the slow development of the MOF-5 shell. The verification of PCN-222@MOF-5 formation was established through optical microscopy pictures. The purple-colored needle-shaped PCN-222 and the colorless cubic MOF-5 confirmed the formation. Citric acid (CA) was utilized to alter the surface of PCN-222 *via* the carboxylate groups in CA, highlighting the importance of post-modification. The synthesis of composites PCN-222@MOF-5 resulted from this, showing that surface functionalization could link two different MOFs. When considering stability, core substrates such as UiO-66(Zr), UiO-67(Zr), PCN-160(Zr), MOF-808(Zr), PCN-222(Zr), PCN-250(Fe), and MIL-125(Ti) were utilized due to their stability as stable MOFs. The series MOF5(Zn), HKUST-1(Cu), and (Yb), which exhibit relatively low stability, were employed as shell MOFs to verify the general applicability of a retrosynthetic stability

assessment. The innovative construction of the MOF@MOF has been successfully achieved, as evidenced by vibrant optical imaging and clear PXRD patterns. This confirms the effectiveness of the approach. Furthermore, modifying the allocation of core and shell MOFs allows for creating various arrangements, including evenly mixed, center-focused, and asymmetric distributions with equal parts. The suggested concepts of altering surfaces and evaluating stability in retrosynthesis are expected to be used in a controlled manner to design and prepare more MOFs@MOFs in the future.<sup>94,105</sup>

### 3. Biomedical applications

MOFs have special characteristics that render them very attractive for use in medical applications. Their porous formations make them ideal for administering various medications. The ability to choose from various metal ions and organic ligands allows for developing MOFs that possess natural anti-tumor properties. This enables the creation of synergistic systems between MOFs and drugs. Furthermore, MOFs can serve as precursors or templates for various anticancer substances.<sup>106</sup> Moreover, controlled preparation methods can lead to the preparation of core-shell structures in MOFs. The original characteristics of MOFs are preserved by these formations, and they also exhibit additional structural characteristics. When MOF core shells are compared to pure MOFs, they contain empty spaces inside, which enables higher drug loading and improved mass transfer capabilities. The combination of MOFs with other functional materials in core-shell structures results in a synergistic effect, where the final outcome exceeds the combined individual components.<sup>107</sup> In this feature article, our focus will be on the utilization of core-shell MOFs in biomedicine, specifically in the fields of bioimaging, biosensing, drug delivery, and synergistic therapy in recent years.

#### 3.1. Bioimaging

Detection and monitoring of lesion areas, as well as the transport of bioactive molecules, are crucial in treating serious diseases like cancer. These aspects rely on diagnostic tools like bioimaging.<sup>107</sup> Bioimaging enables the visualization of an organism's structure, understanding biological functions, and observing biological processes in real-time without physical intervention; it is capable of examining structures at the sub-cellular level up to entire multicellular organisms.<sup>108</sup> Biomedical imaging techniques used in current clinical practices include magnetic resonance (MRI) imaging, computed tomography (CT), and fluorescence (FL) imaging. These techniques can be combined to produce high-resolution images crucial for making informed medical decisions. At the heart of this process are contrast agents. These agents play a pivotal role in differentiating between anatomical variances and enhancing the distinction among bodily tissues, thereby enabling the production of high-quality images that are vital for medical decision-making. Furthermore, contrast agents should have a long enough circulatory duration when administered intravenously. Nanoparticles



(NPs) ranging from 1 to 100 nanometers have proven to be useful tools for imaging inside living organisms for biological diagnosis. They allow for long-term imaging at low doses. MOFs are also seen as potential nanomaterials for bioimaging. These frameworks, which consist of crystalline porous materials composed of inorganic units containing transition metal cations/clusters and connecting organic ligands, offer unique properties that make them suitable for bioimaging applications. Core-shell MOFs with nano-dimensions are utilized as contrast agents for highly effective imaging methods. Their biodegradability enables quick decomposition and cleaning after use. This section will explore the application of core-shell MOF structures in various bioimaging models.<sup>107</sup>

**3.1.1. MRI.** MRI is an imaging technique that detects nuclear spin reorientations in a magnetic field and is noninvasive. It creates anatomical images with excellent spatial resolution and considerable depth of penetration. The method involves using radio-frequency signals produced by the interactions of external magnetic fields or radio waves with the protons (typically from hydrogen atoms) in soft tissues to create detailed images. It captures radio frequency signals from active magnetic cores, particularly hydrogen atoms in the body; hydrogen nuclei are abundant in essential body components such as water and fats, making them widely utilized in MRI. MRI contrast agents come in two types: positive contrast agents that decrease the longitudinal relaxation time ( $T_1$ ) of water protons and damaging contrast agents that diminish the transverse relaxation time ( $T_2$ ) of water protons. Both kinds of MRI contrast agents are accessible for medical use. Contrast agents used in MRI usually consist of chelated transition metal ions such as  $Gd^{3+}$ ,  $Mn^{2+}$ , or  $Fe^{3+}$  to reduce potential side effects. On the other hand,  $T_2$  refers to the transverse relaxation that leads to negative contrast and dark signal contrast; most  $T_2$  contrast agents are superparamagnetic nanoparticles such as  $Fe_3O_4$  nanoparticles.<sup>109–111</sup> Zeng *et al.* created core-shell nanocomposites (NCs) by enclosing PVP-coated gold nanostars (AuNS) inside MIL-101-NH<sub>2</sub>(Fe) (consisting of 2-aminoterephthalic acid as the organic ligand and  $Fe^{3+}$  metal nodes). The nanocomposites were subsequently modified on the surface with a peptide (ZD2) that targets triple-negative breast cancer (TNBC) cells. This led to the formation of AuNS@MIL-101-NH<sub>2</sub>(Fe)-ZD2 structures. The goal was to evaluate the capability of these formations for MRI and PTT in aiming at TNBC tumor cells. The nanocomposites AuNS@MOF-ZD2 showed positive results in  $T_1$ -weighted MR imaging and PTT when tested on nude mice bearing MDA-MB-231 tumors.<sup>111</sup> Fu *et al.* have created a theranostic composite of  $Fe_3O_4$  nanoparticles and UiO-66 with a core-shell structure. The innovative  $Fe_3O_4$ @UiO-66 composites feature a unique core-shell structure that makes them versatile nanocarriers. They have the exciting potential to revolutionize drug delivery while also serving as contrast agents for T2-weighted MR imaging. This dual functionality opens up new possibilities for more efficient treatments and advanced imaging techniques.  $Fe_3O_4$ @UiO-66 demonstrates an impressive ability to load drugs (~63 wt%, 2.0 mg DOX per mg composites) and release them steadily and effectively, establishing it as an outstanding carrier for drug delivery. Its elevated transverse relaxivity ( $255.87 \text{ mM}^{-1} \text{ s}^{-1}$ ) indicates its promise as a contrast

agent for MR imaging. Recent studies reveal some exciting findings about  $Fe_3O_4$ @UiO-66 composites. They boast minimal toxicity and outstanding biocompatibility, making them a promising option in various applications. The research on their cytotoxicity, biodistribution, and *in vivo* toxicology highlights their safe profile, paving the way for innovative solutions in the biomedical field. This opens up exciting possibilities for their potential antitumor effects and MR imaging capabilities in laboratory and living subjects. The treatment with either  $Fe_3O_4$ @UiO-66 or  $Fe_3O_4$ @UiO-66-DOX resulted in promising results, including a high mortality rate of cancer cells, significant inhibition of tumor size, and a noticeable darkening effect in both *in vitro* and *in vivo* studies, offering hope for the future of cancer treatment.<sup>112</sup>

**3.1.2. Computed tomography.** Computed tomography (CT), or X-ray computed tomography, is a non-invasive imaging method that utilizes X-ray attenuation. Various clinical studies use it, and high X-ray attenuation is observed in elements like iodine, barium, and bismuth because of their high atomic numbers (high-Z elements). CT imaging can generate detailed 3D anatomical information and deeply penetrate tissues. It can monitor diseases in various body areas and produce non-invasive 3D tissue images. Small iodinated molecules and suspensions of barium sulfate are commonly used as contrast agents in medical settings. High doses of small molecular contrast agents (CAs) are crucial for enhancing CT imaging resolution. However, owing to their non-specific distribution and impact on blood and lymphatic drainage, this approach may cause side effects, including nausea, reduced blood pressure, and kidney toxicity in certain patients. Understanding these risks is essential for optimizing patient outcomes. Recent progress in core-shell MOFs at the nanoscale has enabled the creation of CT contrast agents using nanotechnology, which possess beneficial characteristics such as minimal toxicity, high X-ray absorption capability, suitable dimensions, and cost efficiency.<sup>107,109</sup> Meng *et al.* employed zirconium metal as a contrast agent in CT imaging to develop a ZIF-8/DOX@ZrO<sub>2</sub>@IL nanocomposite aimed at dual functionality in combined CT-microwave thermal cancer therapy and CT imaging. They created this nanocarrier by wrapping ZrO<sub>2</sub> around ZIF-8 NPs and incorporating DOX while forming ZIF-8 using a simple one-step process. Then, they added an ionic liquid (IL) to the nanocomposite to enhance the efficiency of the microwave thermal treatment. In this configuration, ZrO<sub>2</sub> was chosen as a proficient contrast agent for CT imaging because of its strong X-ray absorption and its capacity to improve the biocompatibility and therapeutic effects of ZIF-8 NPs. The results from CT imaging in mice with H22 tumors indicated that a higher concentration of the nanocomposite improved the CT imaging signals, validating the promise of ZIF-8/DOX@ZrO<sub>2</sub>@IL as a CT contrast agent for *in vivo* diagnostics. The composite demonstrates the integration of CT-imaging-enhancing shells (ZrO<sub>2</sub>) with drug-loaded MOFs and thermally active coatings, supporting the trend of multifunctional theranostic nanoplateforms, and it balances drug release kinetics and heating efficiency while maintaining imaging quality.<sup>113</sup> Zheng *et al.* developed two porous materials to create core-shell nanocomposites aimed at tumor treatment



guided by CT imaging. They employed a one-step method to produce tetra(4-aminophenyl)-21*H*,23*H*-chloride (TAPC), terephthalaldehyde, and PEG5k-NH<sub>2</sub> on the outer shell of amine-modified Hf-UiO-66 (Hf-UiO-AM), yielding Hf-UiO (Fig. 2a). The HUC-PEG nanocomposite that is produced possesses CT and photothermal imaging (PTI) capabilities due to the outstanding X-ray absorption capacity of Hf elements and its remarkable photothermal conversion efficiency (Fig. 2b). In DMF, the FL quantum efficiency of Hf-HUC-PEG and Zr-HUC-PEG is 0.032 and 0.037, respectively. The reduction in tumor weights provides additional evidence of the outstanding antitumor effectiveness of HUC-PEG and the mice's body weights consistently increased during the treatment period, which *in vivo* tests show these results. This research showcases the potential of heavy MOFs involving Hf for dual imaging and therapy. It emphasizes the use of flexible PEG based surface chemistry to enhance tumor accumulation and ensure safety. The study focuses on optimizing the photothermal and fluorescence quantum yields and aims to advance real-time image-guided therapy in deep tissues.<sup>114</sup>

**3.1.3. FL imaging.** FL imaging is a cost-effective technique that generates intricate tissue images by utilizing UV-near infrared (NIR) light to assist in detecting different types of cancer cells. This method can identify early-stage tumors that may not be detected by other imaging techniques using white light or radiation. FL imaging has opened up an exciting world of possibilities by utilizing a wide range of organic and inorganic materials that emit light. This includes captivating fluorophores and striking dye molecules such as porphyrin, phthalocyanine, and cyanine, creating a rich and diverse palette. Additionally, innovative nanosheets, dynamic quantum dots, luminescent

organic ligands, and intriguing metal ions or clusters contribute to their unique glow. While these materials boast impressive FL quantum efficiencies, they have challenges. When introduced into biological environments, their low water solubility and potential changes in chemical structure can significantly diminish their luminescence properties. It's a fascinating yet complex balance between performance and practicality. Conjugating these substances to particular NPs, like polymer-centered NPs and polymeric crosslinked micelles within core-shell MOFs, can tackle these constraints and improve their luminescence characteristics. Integrating fluorescent materials into core-shell MOF structures allows for creating fluorescent nanocomposites (NCs) that can be applied in *in vivo* bioimaging. This method provides benefits like enhanced cellular endocytosis, a significant capability for drug incorporation, and strong biocompatibility, producing top-notch images.<sup>107,108</sup> Wang *et al.* synthesized ICG@ZIF-8 NPs in a single step for the purpose of fluorescence imaging and PTT of tumors. The incorporation of indocyanine green (ICG) into ZIF-8 NPs improved its photothermal stability, increased resistance to photobleaching, and enhanced cell uptake. During laboratory experiments, it was demonstrated that upon exposure to NIR laser irradiation, ICG@ZIF-8 NPs efficiently inhibited SMMC-7721 cells by means of photothermal ablation. Further experiments in living organisms showed that ICG@ZIF-8 NPs were able to accumulate at tumor sites *via* passive targeting, enabling fluorescence imaging of the tumor. Additionally, PTT caused a significant elimination of the tumor. The findings indicate that ICG@ZIF-8 NPs have great potential as theranostic agents for clinical applications because of their straightforward synthesis process, quick production, affordability,



Fig. 2 (a) Creating the HUC-PEG nanocomposite followed by the formation of its MOF-POP and demonstration of the HUC-PEG theranostic platform for conducting CT/photothermal imaging-guided therapy in both *in vitro* and *in vivo* settings. (b) The mechanism of interface-enhanced phototherapy for HUC-PEG. Reproduced from ref. 114 with permission from Elsevier, copyright 2020.



strong photostability, impressive imaging capabilities, and photo-thermal therapy properties.<sup>113</sup> Alijani *et al.* demonstrated a core-shell nanostructure consisting of Fe<sub>3</sub>O<sub>4</sub> as the core and UiO-66-NH<sub>2</sub> MOF as the shell. This nanostructure was loaded with the DOX drug and combined with highly fluorescent carbon dots (CDs). Subsequently, it was linked with the nucleolin-binding Aptamer AS 1411 (Fe<sub>3</sub>O<sub>4</sub>@MOF-DOX-CDs-Apt). Using nucleolin receptor-mediated endocytosis, the researchers could use biocompatible fluorescent carbon dots (CDs) to enter cancer cells. Treating breast cancer cells with the aptamer-conjugated nanostructure revealed bright green FL from carbon dots (CDs) and vibrant red FL from doxorubicin (DOX) within the cells.<sup>115</sup>

### 3.2. Biosensing

A biosensor functions as a device that identifies variations in a biological substance, producing an electrical signal that corresponds to these changes. Biosensor receptors can consist of materials like enzymes, nucleic acids, antigens, and other elements.<sup>116</sup> Biosensors can oversee specific biological processes and identify illnesses by recognizing changes in the signal of particular substances, playing a crucial role in medical treatment.<sup>11</sup> MOFs demonstrate exceptional sensitivity in sensing due to their ability to change color and also offer advantages such as modifiable structures, extensive surface area, porosity, numerous exposed active sites, and outstanding biocompatibility.<sup>117</sup> Moreover, the practical applications of MOFs in improving the binding of antibiotics and biomolecules like glucose, antibodies, and aptamers are significant. Their -NH<sub>2</sub> or -COOH functional groups have been successfully utilized as frameworks, and their core-shell configurations offer further promise for biosensor uses by enhancing optical characteristics, durability, and selectivity.<sup>93,118</sup> Creating advanced and innovative biosensors that provide effective detection beyond traditional methods is currently a difficult task.<sup>119</sup> Liu *et al.* enhanced a uniform voltammetric (HVC) sensor using an electrochemical approach to identify Pb<sup>2+</sup>. The Me@UiO-66-NH<sub>2</sub> system functions as the responsive material prompted by the smart target. The UiO-66-NH<sub>2</sub> MOF, serving as a nanocarrier, encapsulates a signal probe (methylthionine chloride) and is coated with COOH complementary sequences (CP) and Pb<sup>2+</sup> aptamers. The HVC sensor optimized with Me@UiO-66-NH<sub>2</sub> shows remarkable analytical performance under specific conditions. It displays exceptional analytical abilities with a minimal limit of detection (LOD) of 0.166 pM and a wide linear range from 5.0 pM to 500.0 nM. These findings demonstrate a low LOD and an extensive linear range, highlighting superb analytical performance. This MOF framework serves as a signal transmitter and a ground-breaking platform for creating aptamer-based bioelectronic devices boasting remarkable sensitivity. It preserves selectivity within intricate sample matrices and has the potential for multiplex detection. Incorporating this pioneering MOF-aptamer system into portable sensors facilitates on-site monitoring of heavy metals in water and guarantees food safety.<sup>120</sup> Lu *et al.* created a composite material called UiO-67@Ni-MOF and utilized it to detect glucose. They proved the formation of the mentioned structure with SEM, TEM, and EDS elemental mapping analyses (Fig. 3b and c). The impressive surface area and robust electrocatalytic capabilities of UiO-67 significantly

boosted electron transfer in UiO-67@Ni-MOF, enhancing its performance and efficiency. In addition, the Ni-MOF showed remarkable electrochemical catalytic capabilities for glucose, making it a standout performer in the field. The results of the amperometry test indicated that when conditions were optimal, the sensor demonstrated quick response (under 5 seconds), a wide linear range (5 mM to 3.9 mM), and a low detection limit (0.98 mM). Furthermore, it demonstrated remarkable consistency, boasting a relative standard deviation of just 1.1%, alongside an impressive overall reliability with a relative standard deviation of 1.9%. Plus, it showcased exceptional durability over time. The developed electrochemical biosensor demonstrated rapid response times, a broad detection range, and a low limit of detection (LOD) (Fig. 3a).<sup>121</sup>

### 3.3. Drug delivery systems

The current era sees both cancer and bacterial illnesses posing a significant danger to human health, emphasizing the continuous necessity for research, public health campaigns, and advancements in healthcare. The targeted transportation of drugs for these illnesses has become a crucial challenge. Throughout history, drugs have played an essential role in combating diseases, and the continuous advancement of science and technology has led to the creation of increasingly effective drugs. Nonetheless, the adverse effects of drugs and their breakdown in the body's environment significantly impede their clinical usage. To overcome this hurdle, the use of nanocarriers, which can load and release drugs at specific sites within the body, has been proposed and demonstrated as an effective treatment strategy.<sup>110</sup> The nanoscale core-shell MOF structures have high porosity and a large surface area, which make them potential drug carriers. MOFs' molecularly precise porous structure and organic-inorganic hybrid nature provide them with unique adsorption properties, making core-shell MOFs ideal for drug loading. MOFs can effectively deliver drugs with varying molecular weights, hydrophilicity, and sizes at predetermined ratios.<sup>106</sup> Here, we address the significance of drug delivery in the individual treatments of cancer and bacterial diseases.

**3.3.1. Cancer therapy.** Treatment of cancer, a worldwide concern, involves fighting the uncontrolled growth of cells, their ability to metastasize to other areas of the body, and damage to bodily tissues and organs, often leading to death. Traditional cancer treatments, like chemotherapy, can result in the destruction of healthy cells as well as cancerous ones, causing side effects. As a result, new therapeutic approaches and methods for delivering drugs have been developed in recent years.<sup>21</sup> MOFs have been successfully employed as nanoplat-forms to treat cancer. Smart core-shell MOFs have the ability to detect and respond to changes in the environment and external triggers, showing predictable changes in physical and chemical properties. Stimuli can be divided into endogenous (*e.g.*, pH and biomolecules) and exogenous (*e.g.*, light and magnetic field) categories.<sup>122</sup> Significant effort has been dedicated to developing multifunctional theranostic nanomedicine platforms, including versatile diagnostic and therapeutic systems based on core-shell



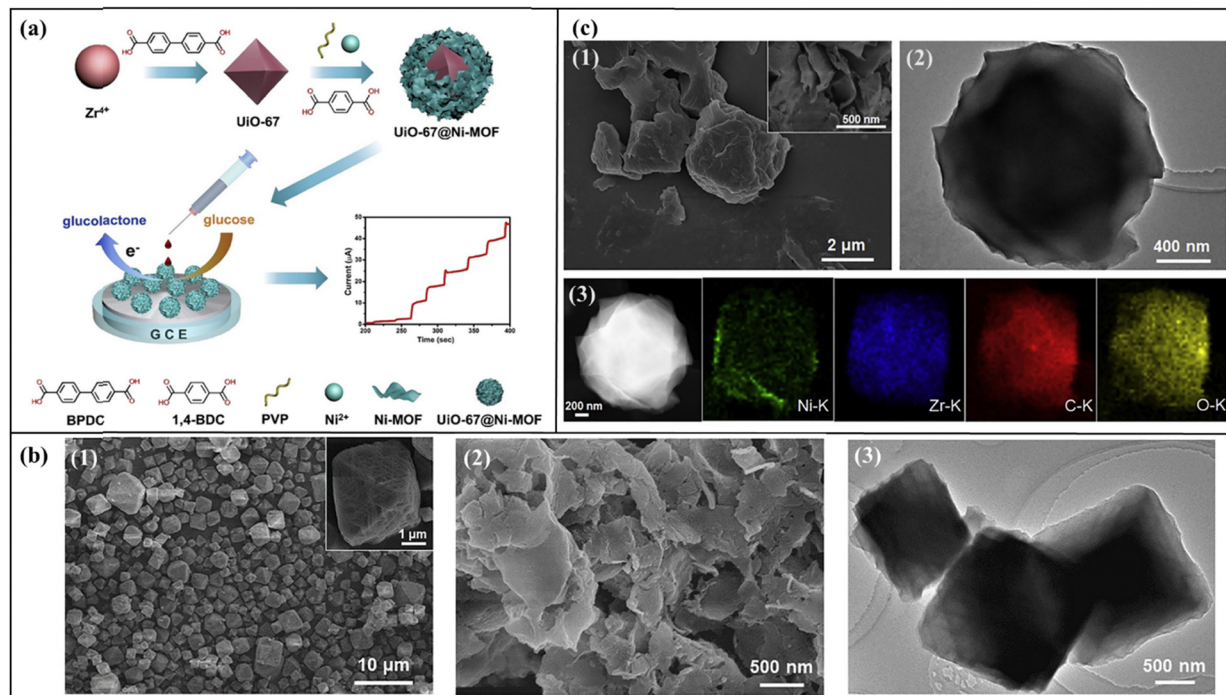


Fig. 3 (a) Illustration provided in the schematic shows the process of creating core-shell UiO-67@Ni-MOF composites through internal extended growth while being regulated by polyvinylpyrrolidone. The modified electrode with UiO-67@Ni-MOF is used for nonenzymatic glucose sensing. (b) (1) SEM images of UiO-67, (2) Ni-MOF, and (3) TEM images of UiO-67. (c). (1) SEM image, (2) TEM image, and (3) EDS elemental mapping of prepared UiO-67@Ni-MOF. Reproduced from ref. 121 with permission from Elsevier, copyright 2020.

MOFs, to achieve improved antitumor effectiveness.<sup>123</sup> MOFs with a core-shell structure exhibit high-quality material properties, good water stability, and versatility for various treatment methods such as drug delivery, light therapy, and photodynamic therapy, offering great potential for cancer treatment.<sup>124</sup> Taheri-Ledari *et al.* conducted a comparison of exploring the innovative world of core/shell and surface composite architectures as part of their characterization process. The core/shell architecture outperforms the surface composite architecture in terms of structural stability, magnetic properties, surface area, and porosity characteristics. The researchers investigated the effectiveness of a highly efficient drug delivery system created using Fe<sub>3</sub>O<sub>4</sub> NPs and Bio-MOF-13. DOX, a widely recognized cytotoxic substance, was incorporated into the cavities to create the composite DOX@Fe<sub>3</sub>O<sub>4</sub>/Bio-MOF-13, in order to assess the effectiveness of the Fe<sub>3</sub>O<sub>4</sub>/Bio-MOF-13 drug delivery system. Their research, utilizing confocal microscopy and flow cytometry, demonstrated a significant rise in the discharge of DOX from the core/shell arrangement within upon the application of an external magnetic field; the nucleus and cytoplasm of MDA-MB-231 cells respond in fascinating ways. The core/shell structure showed minimal DOX release in blood serum pH and maximum release within the internal environment of cancer cells. The final composite has high toxicity for MDA-MB-231 cells, while the carrier's components have low toxicity, thus confirming the safety of the structure. The findings indicate that the core/shell composite DOX@Fe<sub>3</sub>O<sub>4</sub>/Bio-MOF-13 has the potential to be a favorable choice for effective, affordable, and safe treatment of breast cancer.<sup>122</sup> Zhao *et al.* found that integrating medical

diagnosis and treatment shows potential by combining heterostructures of lanthanide-doped upconversion nanoparticles (DUCNPs) and MOFs. The team created the DUCNP@Mn-MOF nanocarrier, which can efficiently load and transport a cytotoxic antitumor drug known as 3-F-10-OH-evodiamine (FOE). The system DUCNP@Mn-MOF/FOE takes advantage of the pH-responsive and peroxidase-like characteristics of the Mn-MOF and the distinctive optical properties of DUCNPs to create hemodynamic and chemotherapeutic effects in a synergistic manner (Fig. 4a). The team managed to overcome the inherent limitations of FOE by utilizing the DUCNP@Mn-MOF nanocarrier. This allowed them to address issues related to FOE's unfavorable physicochemical properties of this compound, which are quite intriguing, but its *in vivo* potency is somewhat limited. They displayed live FL imaging of mice with tumors in the right hind leg after receiving different treatment groups (Fig. 4c). This intricate nanosystem reacts with the tumor microenvironment and demonstrates superb tumor-targeting ability. DUCNP@Mn-MOF/FOE offers significant potential for cancer treatment due to its ability to deliver drugs in a highly selective and bioavailable manner. In a model of breast cancer in mice, DUCNP@Mn-MOF/FOE efficiently suppressed tumor growth with no notable toxicity (Fig. 4b). As a result, this suggested that this nanosystem shows excellent promise as a theragnostic platform for the combined diagnosis and treatment of tumors using multiple methods, instilling hope for its future applications.<sup>125</sup>

**3.3.2. Antibacterial drug delivery.** Over the last ten years, there has been a concerning rise in bacteria developing resistance to antibiotics. This problem has been worsened by the



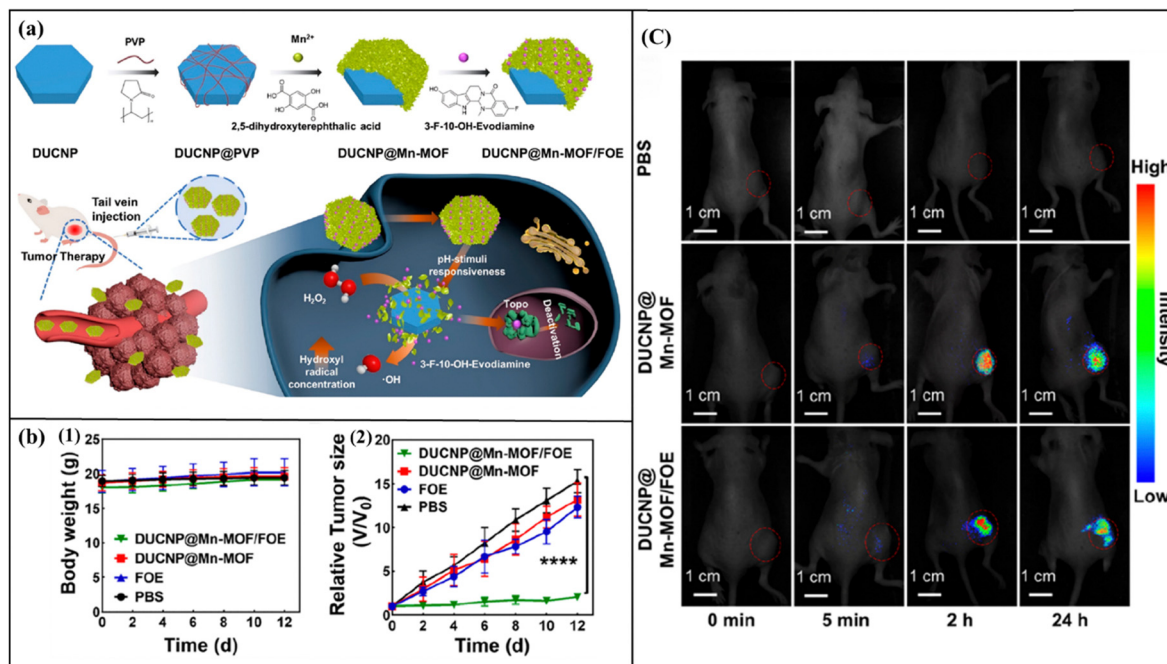


Fig. 4 (a) Designing a DUCNP@Mn-MOF framework for the multifaceted fusion therapy of cancer and understanding how the nanoparticles (DUCNP@Mn-MOF/FOE) hinder the growth of tumor cells. (b) (1) Body weight changes in mice. (2) Using DUCNP@Mn-MOF/FOE treatment leads to successful inhibition of tumor growth in living organisms. The tumor volumes for each group ( $n = 5$ ; \*\*\*\* $p < 0.0001$ ) were examined. (c) *In vivo* FL imaging was conducted on mice bearing tumors in their right hind leg following various administration groups. Reproduced from ref. 125 with permission from American Chemical Society, copyright 2023.

slower advancement in the research and creation of new antibiotics compared to the rapid development of resistance by disease-causing bacteria. To tackle this issue, alternative treatment methods need to be considered instead of traditional antibiotics. For instance, materials such as MOFs in core-shell structures have desirable characteristics such as improved internalization by bacteria, flexible control over structure, high selectivity, and regulated drug release. As a result, these materials display potential as possible options for addressing antibiotic resistance and could present new opportunities for antibacterial treatment.<sup>126,127</sup> Tu *et al.* synthesized cubic-shaped ZIF-8 nanoparticles. The chemically inactive sites of cubic ZIF-8 and the hydrophobic CTAB attached to the surface helped to reduce the issue of self-etching during the polydopamine (PDA) coating. The core-shell ZIF-8@PDA particles were prepared successfully, and most of the ZIF-8 templates remained intact. In physiological buffers, the release of  $Zn^{2+}$  from ZIF-8@PDA due to degradation exhibited a distinct pattern that depended on the pH. In the initial stage, there was limited and pH-independent release of  $Zn^{2+}$ , followed by a subsequent rapid release stage. ZIF-8@PDA showed improved antibacterial properties against *S. aureus*, mainly by disrupting the bacterial membrane. The scientists propose that this method could potentially be used with other nanoparticles that release metal ions and may be improved for potential use inside living organisms. Incorporating metal-ion-releasing nanoparticles like  $Ag^+$  and  $Cu^{2+}$  greatly enhances the range of antimicrobial uses. This research introduces a new approach for self-etching prevention that employs CTAB and PDA,

creating stable MOF-based antimicrobial agents suitable for biological settings.<sup>128</sup> Huang *et al.* successfully developed a nano-theranostic agent named  $ONP@ZnO_2@ZIF-67$ . It is approximately 110 nm in size and has a core-shell structure with a spherical shape. This agent was designed to detect and eliminate bacteria simultaneously. The changes in FL signals were observed to verify the interaction of  $ONP@ZnO_2@ZIF-67$  with a biomarker for bacterial infection,  $ONOO^-$ . This interaction led to the generation of fluorescent MB dye, effectively detecting bacteria (Fig. 5b-d). Additionally,  $ZnO_2$  was utilized to provide  $O_2$  and  $H_2O_2$ , and the acidic environment caused the outer layer of ZIF-67 to break down. This breakdown of  $H_2O_2$  produces potent hydroxyl radicals, known for their significant toxicity to biological organisms and ability to eliminate bacteria in response to pH changes effectively. Furthermore, the resultant MB aids in converting the generated  $O_2$  into singlet oxygen, further enhancing the elimination of bacteria (Fig. 5a). The  $ONP@ZnO_2@ZIF-67$  nanomedicine was shown to reduce infection-induced inflammation and speed up the healing of wounds in *in vivo* experiments. This advanced nano-theranostic agent is a potent antibacterial remedy integrating infection identification and bacterial elimination by synergistically boosting CDT and PDT.<sup>129</sup>

### 3.4. Synergistic therapy

Nowadays, research is concentrating on creating multimodal treatment approaches to achieve better antitumor results. Conventional cancer treatments like surgery, radiation, and chemotherapy can be life-saving, but they often come with a



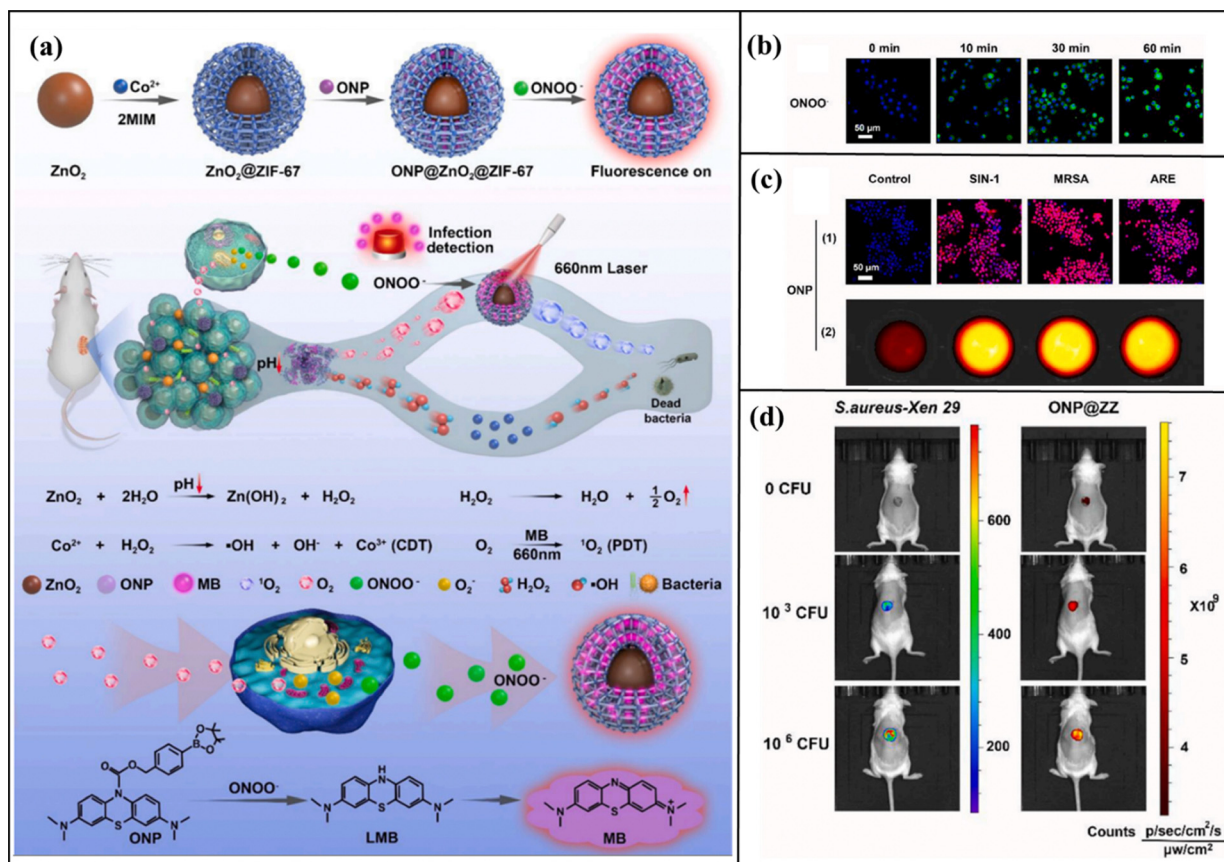


Fig. 5 (a) Preparation of ONP@ZnO<sub>2</sub>@ZIF-67 and understanding how the nanosystem works for identifying and treating infections. (b) Macrophages expressed ONOO<sup>-</sup> after being infected with methicillin-resistant *Staphylococcus aureus* (MRSA) at various time points. (c) Images of FL signals from macrophages stimulated by 3-morpholino sydnonimine hydrochloride (SIN-1, ONOO<sup>-</sup> donor), MRSA, and antibiotic-resistant *Escherichia coli* (ARE) were captured. (1) Seen using a confocal laser scanning microscope. (2) Viewed using an *In vivo* imaging system (IVIS). (d) The FL intensity of probes is used to assess the level of bacterial infection at wound locations. Reproduced from ref. 129 with permission from Elsevier, copyright 2022.

harsh price. Patients frequently face a whirlwind of side effects, grapple with high rates of recurrence, and even develop resistance to multiple drugs.<sup>130</sup> As a growing method for treating cancer, combined therapy using core-shell MOFs, which involves multiple models of phototherapy, has gained considerable interest because of its minimal side effects, inherent non-invasiveness, and precise targeting when the tumor sites are exposed to localized radiation. The combination of various medical treatments in synergistic cancer therapy has demonstrated improved therapeutic outcomes and significantly decreased toxicity compared to individual therapy.<sup>131</sup> In the fight against cancer, use of core-shell MOFs in biomedicine has become a hopeful and advanced method for delivering drugs or cargo. Their exceptional characteristics, including efficient loading of drugs/cargo and degradation triggered by the tumor microenvironment, have given rise to optimism within the medical field. Core-shell MOFs, particularly those that combine several theranostic components, have substantial promise for effective cancer therapy.<sup>132</sup> MOFs provide significant benefits for creating versatile treatment platforms due to their adjustable structure and expansive surface area. Exploring different combinations of therapies using MOF core-shell

structures, such as chemo/photodynamic therapy, chemo/photothermal therapy, photothermal therapy/photodynamic therapy, and chemo/photothermal therapy/photodynamic therapy, has demonstrated encouraging therapeutic outcomes for treating tumors. This part will explore the most recent example of combined therapy using MOF core-shell structures.<sup>21</sup>

**3.4.1. Chemo/PDT.** PDT proves to be a successful anti-cancer treatment. PDT is a type of phototherapy that utilizes three non-harmful elements – a photosensitizer (PS), a source of light, and tissue oxygen – to cause harm to malignant and other irregular cells. The performance of the PDT method uses light; the light-activated photosensitizer (PS) interacts with oxygen and other molecules in the tissue, leading to the creation of reactive oxygen species (ROS), especially singlet oxygen (<sup>1</sup>O<sub>2</sub>). This causes cellular toxicity and harms proteins and organelles, facilitating the accumulation of anticancer drugs in tumor cells.<sup>132</sup> PDT can potentially eliminate diseased tissues precisely by utilizing the specific absorption of the photosensitizer and localized exposure to light, presenting a minimally invasive method for treating cancer. The core-shell structure of the MOF demonstrates exceptionally high photosensitizer loading. This category of MOF frameworks have



emerged as an innovative generation of photosensitizers and have displayed remarkable results in preclinical studies.<sup>133–135</sup> The core-shell compounds' porous MOF structure enables drug incorporation. It also facilitates the smooth diffusion of reactive ROS, like  $^1\text{O}_2$ , from the core-shell MOF interior to exert their cytotoxic impact on cancer cells.<sup>136</sup> Li *et al.* created a core-shell upconversion nanoparticle@porphyrinic MOF (UCSSs) to overcome these limitations by combining chemo/PDT. The core of the upconversion nanoparticle (UCNP) absorbs NIR light, which can penetrate tissue. It then transfers this energy to the porphyrins in the MOF shells, enabling efficient singlet oxygen generation when exposed to NIR light. Furthermore, a hypoxia-activatable prodrug, tirapazamine (TPZ), was placed in the nanopores of the MOF (TPZ/UCSSs) to create toxic oxidizing radical species in a low-oxygen (hypoxia) environment. This system has been developed as a promising method to enhance cancer treatment in laboratory settings (*in vitro*) and within living organisms (*in vivo*). This is accomplished through a combination of NIR light-induced PDT and hypoxia-activated chemotherapy, demonstrating the potential to induce anti-tumor therapy effectively.<sup>127</sup> Ding *et al.* have enhanced the design and development of a novel multifunctional platform having a core-shell structure known as 5-ALA@UiO-66-NH-FAM@CP1 (ALA = 5-aminolevulinic acid, CP1 = zirconium-pemetrexed (Zr-MTA)). In this platform, CP1 serves as the shell and is encompassed within UiO-66-NH<sub>2</sub>, forming a core-shell structure. This arrangement improves the high loading rate of MTA because of the strong attraction between MTA and the unsaturated Zr site of UiO-66-NH<sub>2</sub> (Fig. 6b). Additionally, 5-ALA and 5-carboxyl fluorescein (5-FAM) have been successfully loaded and covalently linked with UiO-66-NH<sub>2</sub> due to its high porosity and the presence of amino groups. The analysis findings suggest that the platform demonstrates a superior MTA loading rate (41.03 wt%) compared to previously documented values. This substance has shown remarkable anti-cancer properties

when combined with chemotherapy and PDT, outperforming the effectiveness of each treatment on its own. The results from both laboratory and animal studies also indicate strong folate-targeting capabilities and the achievement of highly effective anti-cancer actions through combined chemotherapy.<sup>137</sup> So combined chemo/photodynamic therapy could overcome these drawbacks and improve the efficiency of cancer treatment.<sup>133,134</sup>

**3.4.2. Chemo/PTT.** PTT uses materials known as photothermal agents (PTAs) with high photothermal conversion efficiency to transform light energy, typically near-infrared light, into heat. This localized overheating destroys cancer cells. The most effective photosensitizers and PTAs should be minimally toxic, a high absorbent of NIR light, and display high photostability. Once injected into the body, these specialized agents employ advanced recognition methods to zero in on tumor tissue, delivering highly accurate and targeted treatment. When subjected to an outside source of light, usually in the near-infrared range, they harness light energy, converting it into heat to effectively target and eliminate cancer cells without needing a photosensitizer to absorb photons and create oxidation-active molecules. Combining photothermal reagents and MOF materials offers a new approach to treating tumors. Core-shell MOF materials are frequently utilized as carriers for PTAs in PTT due to their exceptional performance. The photothermal reagents generate heat when stimulated by external lasers to thermally destroy tumors, while MOF materials have FL properties that enhance the combined therapeutic and diagnostic effects for cancer treatment. However, completely eradicating solid tumors using PTT alone is difficult. Therefore, combining PTT with other treatment methods allows for leveraging the advantages of each process, resulting in additional or synergistic therapeutic effects. MOFs are 3D compounds made of metal ions and organic molecules with permanent porosity, making them a versatile platform to load various functional components for specific applications. Recently, various photothermal nanomaterials have



Fig. 6 (a) Schematic diagram depicting the preparation of ICG-PFH/MOF/DNA-DOX and the mechanism of synergistic photo-chemotherapy. Reproduced from ref. 138 with permission from Elsevier, copyright 2024. (b) The strategy of synthesis and chemotherapy are integrated with PDT in the UiO-66-NH<sub>2</sub>. Reproduced from ref. 137 with permission from Elsevier, copyright 2022.



been incorporated into organic ligands to combine their unique photothermal effects with the benefits of core-shell MOFs, ultimately enhancing their performance for cancer therapy. This approach achieves the distinctive structural properties of MOFs and significantly enhances the therapeutic efficiency of phototherapy on tumors, contributing to additional or synergistic effects.<sup>21,131,139–141</sup> Zhaojie *et al.* created the CuS@Fe MOF-DOX nano platform, which shows enhanced absorption of NIR light and improved photothermal efficiency. This is achieved by leveraging the localized surface plasmon resonance (LSPR) effect of CuS and the nanoscale MOFs. These materials have garnered attention as carriers for drugs in biomedical applications due to their high capacity for loading drugs and enzymes, ease of adaptability for multimodal imaging, and ability to degrade to minimize long-term toxicity. The CuS@Fe-MOF-DOX nano platform exhibits strong absorption of NIR light, efficient conversion of photothermal energy, loading of DOX, responsive release based on pH, MRI capabilities, and good compatibility with living organisms. This platform enables inhibition and destruction of tumors through a combination of photothermal and chemotherapy, which is significantly more effective than using either treatment alone.<sup>142</sup> Li *et al.* described a versatile nano-thermal therapy platform known as Fe<sub>3</sub>O<sub>4</sub>-NH<sub>2</sub>@Au@MIL101-NH<sub>2</sub>. This platform comprises magnetic iron oxide nanoparticles, dopamine (PDA), gold nanocages (Au nanocages), and a MOF, MIL-101-NH<sub>2</sub>, for simultaneous chemotherapy treatment of tumors in both laboratory settings and living organisms. The developed magnetic photothermal nanoparticles (MPNPs) possess a high capacity for drug loading, exceptional photothermal ability, low biotoxicity, perfect NMR, and significant *in vivo* anti-tumor impact. The innovative and versatile nano platform has great potential for targeted tumor synergy therapy. The substantial adhesion property of PDA allows Au nanocages to bind to Fe<sub>3</sub>O<sub>4</sub>-NH<sub>2</sub> nanoparticles, creating Fe<sub>3</sub>O<sub>4</sub>-NH<sub>2</sub>@Au nanostructures quickly. Adding Au nanocages to PDA significantly improves the photothermal properties of MPNPs. The outer layer of MIL101-NH<sub>2</sub> does not affect the photothermal characteristics of Fe<sub>3</sub>O<sub>4</sub>-NH<sub>2</sub>@Au@MIL101-NH<sub>2</sub>, while demonstrating exceptional drug-loading capabilities. Our findings clearly show that the low toxicity of MPNPs *in vivo* significantly enhances both chemotherapy and photothermal therapy, effectively treating and eradicating tumors.<sup>143</sup>

**3.4.3. PTT/PDT.** Light-based therapies for tumors are receiving increased attention due to their perceived advantages, such as minimal invasiveness, precise targeting, and reduced side effects. PDT and PTT are two well-known types of light-based treatments that have become important tools for tumor therapy. There is increasing interest in combining PDT and PTT to achieve a more effective treatment. These two methods are the main non-invasive light-based therapies used in medical practice. It has been observed that the combination of PDT and PTT leads to significantly improved efficacy, as the appropriate level of heat can enhance blood flow within the tumor, increasing the delivery of oxygen molecules and thus improving the effectiveness of PDT. Investigators have recently explored a core-shell MOF as a flexible foundation for integrating PDT and PTT, two innovative, noninvasive, light-activated treatments that create a

synergistic effect that boosts their effectiveness while minimizing side effects.<sup>132</sup> Lei *et al.* developed a highly adaptable nanohybrid by combining MIL-101 with black phosphorus BQ to create a novel platform for cancer treatment using PTT and PDT. The BQ was carefully encapsulated within MIL-101, and then catalase was loaded onto the outer layer. Additionally, folic acid-conjugated polyethylene glycol (FA-PEG) was applied to the surface of the BQ-MIL@cat-MIL nanoplatfrom to facilitate targeted delivery to cancer cells. Upon internalization by tumor cells, the nanoplatfrom BQ-MIL@cat-fMIL utilized catalase to convert hydrogen peroxide (H<sub>2</sub>O<sub>2</sub>) into oxygen (O<sub>2</sub>). This generated O<sub>2</sub> was then directed to the inner part of the nano-platfrom to produce 1O<sub>2</sub>, effectively mitigating tumor hypoxia and significantly enhancing the efficacy of PDT.<sup>144</sup> As previously mentioned, the effectiveness of combining PTT and PDT can be significantly enhanced when multimodal imaging is used for tumor diagnosis. Zhou *et al.* conducted research on AuNR@MOF core-shell heterostructures consisting of a single AuNR at the center and mesoporous porphyrinic MOFs making up the external shell. The study focused on the distinct function of the porphyrinic MOF shell, which plays a vital role in producing photoinduced singlet oxygen. The characteristic of AuNRs in plasmonic photothermal conversion is evident when combined, these core-shell heterostructures show promise in combined PDT and PTT against tumors. The mesoporous structure of the heterostructures further improves their effectiveness. AuNRs are commonly used as photothermal agents due to their outstanding photothermal conversion capability. By combining porphyrinic MOFs with plasmonic gold nanorods (AuNRs) into a unified heterostructure, this approach utilizes targeted light capture. This innovative fusion enhances photothermal conversion and increases the generation of singlet oxygen. The AuNR@MOFs show more robust effectiveness in fighting tumors than PDT or PTT alone, both *in vitro* and *in vivo*.<sup>145</sup>

**3.4.4. Chemo/PTT/PDT.** The simultaneous use of various anticancer therapies, such as chemo, PTT, and PDT, within a core-shell MOF with exclusive physical and chemical characteristics, has shown great promise in achieving strong anti-cancer results and lowering the risk of cancer recurrence. The incorporation of chemo/PTT/PDT has garnered attention due to the following advantages: (1) photothermal agents generate heat to enhance blood flow, leading to increased oxygen delivery to the tumor and improving the effectiveness of PDT. (2) The synergistic impact of PDT/PTT enhances the body's ability to fight against tumors.<sup>146,147</sup> Jin *et al.* have described a simple approach for utilizing gold nanorods that have been functionalized and can be used as seed crystals to grow MOFs, resulting in the production of porphyrinic MOF-coated gold nanorods (AuNR@MOFs) that serve as a combined diagnostic and therapeutic platform. The selected porphyrinic MOF, Zr6(TCPP)1.5, comprises a 6-connected Zr6 cluster and a tetra-atomic linker TCPP. Porphyrinic MOFs have distinct characteristics originating from the porphyrin building blocks and demonstrate significant promise in cancer treatment, detection, and light emission. These MOFs can deliver medication and stabilize metal nanostructures because of their precisely defined pore structures and extensive surface areas. Camptothecin (CPT)



is employed as a prototype drug because of the large surface area of porphyrinic MOFs, ensuring a high drug-carrying capacity. The MOFs containing porphyrin enable PDT and FL emission, giving AuNR@MOFs theranostic capabilities. This set of features allows AuNR@MOFs to demonstrate improved efficiency in loading drugs, releasing drugs induced by NIR light, and imaging using FL. Furthermore, it can produce reactive species through photothermal activity to treat cancer in combination. The AuNR@MOFs@CPT photothermal effect can cause local hyperthermia when exposed to NIR light to eradicate tumor cells without requiring a low-oxygen environment. Local hyperthermia increases blood flow, enhancing oxygen supply and improving the combined effect with photodynamic therapy. The cell membrane's permeability is also raised, and it accelerates the release of CPT from AuNR@MOFs@CPT, causing a quick release of CPT within the tumor and increasing chemotherapy cytotoxicity. Additionally, combining chemotherapy, photothermal-triggered CPT release, and PDT can boost each other, enhancing antitumor effectiveness and decreasing the chances of tumor recurrence.<sup>148</sup> Lin *et al.* have created a unique nano-platform (ICG-PFH/MOF/DNA-Dox) intended for targeted FL imaging-guided photo-chemotherapy and managing the hypoxic tumor environment during cancer therapy. This platform employs a MOF as a nucleus for storing indocyanine green (ICG) and perfluorobutane (PFH). It utilizes double-stranded nucleic acids (dsDNA) as an outer layer containing ATP aptamer and AS1411 aptamer and functions as a DOX binding site. ICG-PFH/MOF/DNA-Dox demonstrates targeted recognition of tumor cells by binding to nucleolin receptor sites on cancer cell membranes. This results in the precise release of DOX in the mitochondria, facilitated by ATP-induced dsDNA dissociation, for chemotherapy (Fig. 6a). When ICG is exposed to a single laser, it functions as a photothermal agent, producing heat for PTT, and as a photosensitizer, generating reactive oxygen species to conduct PDT of tumors. When loaded with PFH, it is an autonomous O<sub>2</sub> provider for relieving hypoxia during PDT and chemotherapy. Significantly, the heat generated from PTT also assists in melting dsDNA to speed up Dox release, thereby improving chemotherapy effectiveness. ICG-PFH/MOF/DNA-Dox shows an impressive ability to inhibit tumor growth in both laboratory and living systems by using a combination of PTT/PDT/CT that is relieved under hypoxic conditions.<sup>138</sup>

## 4. Conclusion and perspectives

Core-shell MOFs represent an exciting and versatile class of materials with significant potential for biomedical applications. The core-shell design allows for precise tailoring of their structures, compositions, and functionalities, resulting in improved control over their physicochemical properties, including stability, biocompatibility, and targeted delivery. Recent advancements in synthetic methodologies such as one-pot synthesis, *in situ* synthesis, post-synthetic modification, LBL assembly, self-templating, and epitaxial growth have expanded the capabilities of core-shell MOFs. These innovations enable their application

in various biomedical applications, including drug delivery, bioimaging, biosensing, and synergistic therapy.

Despite their significant potential, several challenges must be addressed before core-shell MOFs can be widely used in clinical applications. Key issues include large-scale production, reproducibility, and long-term biocompatibility, all of which require further investigation. Additionally, the potential toxicity of certain metal components and their degradation products must be carefully evaluated through rigorous preclinical studies. It is also essential to understand how these materials interact with biological systems at the molecular and cellular levels in order to optimize their safety and effectiveness.

Looking ahead, integrating advanced computational modeling and machine learning into the design of core-shell MOFs could accelerate the discovery of novel structures specifically tailored for biomedical applications. Additionally, interdisciplinary collaborations among materials scientists, chemists, biologists, and clinicians will be essential for overcoming current limitations and fully realizing the potential of these materials in precision medicine. With ongoing research efforts and technological innovation, core-shell MOFs have the potential to transform the field of biomedical engineering and enhance healthcare outcomes worldwide.

## Data availability

No primary research results, software or code have been included and no new data were generated or analysed as part of this review.

## Conflicts of interest

There are no conflicts to declare.

## Acknowledgements

The authors acknowledge the partial support from the Research Council of the Iran University of Science and Technology (IUST).

## References

- O. M. Yaghi, G. Li and H. Li, *Nature*, 1995, **6558**, 703–706.
- H. Li, M. Eddaoudi, M. O'Keeffe and O. M. Yaghi, *Nature*, 1999, **6759**, 276–279.
- S. Ibrar, N. Z. Ali, E. O. Ojegu, O. B. Odia, L. Ikhioya and I. Ahmad, *Appl. Organomet. Chem.*, 2023, **3.4**, 294–307.
- G. Cai, P. Yan, L. Zhang, H. C. Zhou and H. L. Jiang, *Chem. Rev.*, 2021, **20**, 12278–12326.
- N. Zhang, B. Zhu, F. Peng, X. Yu, Y. Jia, J. Wang, L. Kong, Z. Jin, T. Luo and J. Liu, *Chem. Commun.*, 2014, **50**(57), 7686–7689.
- K. Koh, A. G. Wong-Foy and A. J. Matzger, *Chem. Commun.*, 2009, 6162–6164.
- K. A. McDonald, J. I. Feldblyum, K. Koh, A. G. Wong-Foy and A. J. Matzger, *Chem. Commun.*, 2015, **60**, 11994–11996.



- 8 O. Kwon, J. Y. Kim, S. Park, J. H. Lee, J. Ha, H. Park, H. R. Moon and J. Kim, *Nat. Commun.*, 2019, **10**(1), 3620.
- 9 E. Ozyilmaz, O. Caglar, I. Sargin and G. Arslan, *Mater. Today Commun.*, 2022, **30**, 103066.
- 10 V. Shrivastav, P. Dubey, S. Sundriyal, U. K. Tiwari and A. Deep, *Coord. Chem. Rev.*, 2024, **499**, 215497.
- 11 X. Ge, R. Wong, A. Anisa and S. Ma, *Biomaterials*, 2022, **281**, 121322.
- 12 M. X. Wu, J. Gao, F. Wang, J. Yang, N. Song, X. Jin, P. Mi, J. Tian, J. Luo, F. Liang and Y. W. Yang, *Small*, 2018, **14**(17), 1704440.
- 13 J. Yang, D. Dai, X. Zhang, L. Teng, L. Ma and Y. W. Yang, *Theranostics*, 2023, **13**(1), 295.
- 14 M. X. Wu and Y. W. Yang, *Adv. Mater.*, 2017, **29**(23), 1606134.
- 15 P. Shams, H. Panahi, M. Tahan, F. Jahansooz and A. Heidaripour, *J. Med. Nanomater. Chem.*, 2023, 267–275.
- 16 J. Gao, H. M. Yu, M. Wu, Q. Chen, Y. Yang, Y. Qu, M. Sun, J. C. Qin, L. Ma and Y. W. Yang, *Mater. Today Chem.*, 2022, **23**, 100716.
- 17 J. Yang, D. Dai, Z. Cai, Y. Q. Liu, J. C. Qin, Y. Wang and Y. W. Yang, *Acta Biomater.*, 2021, **15**(134), 664–673.
- 18 M. X. Wu, H. J. Yan, J. Gao, Y. Cheng, J. Yang, J. R. Wu, B. J. Gong, H. Y. Zhang and Y. W. Yang, *ACS Appl. Mater. Interfaces*, 2018, **10**(40), 34655–34663.
- 19 M. Sajjadnejad and S. M. Haghshenas, *J. Med. Nanomater. Chem.*, 2023, 69–91.
- 20 W. J. Rieter, K. M. L. Taylor and W. Lin, *J. Am. Chem. Soc.*, 2007, **129**(32), 9852–9853.
- 21 J. Tang, C. Huang, Y. Liu, T. Wang, M. Yu, H. Hao, W. Zeng, W. Huang, J. Wang and M. Wu, *Coord. Chem. Rev.*, 2023, **490**, 215211.
- 22 H. Shen, J. Liu, J. Lei and H. Ju, *Chem. Commun.*, 2018, **66**, 9155–9158.
- 23 J. Yang and Y. W. Yang, *Small*, 2020, **16**(10), 1906846.
- 24 M. Liu, Z. Xing, Z. Li and W. Zhou, *Coord. Chem. Rev.*, 2021, **446**, 214123.
- 25 J. W. Osterrieth, D. Wright, H. Noh, C. W. Kung, D. Vulpe, A. Li, J. E. Park, R. P. Van Duyne, P. Z. Moghadam, J. J. Baumberg and O. K. Farha, *J. Am. Chem. Soc.*, 2019, **141**(9), 3893–3900.
- 26 L. Wang, D. Jia, L. Yue, K. Zheng, A. Zhang, Q. Jia and J. Liu, *ACS Appl. Mater. Interfaces*, 2020, **12**(42), 47526–47538.
- 27 P. Parnicka, W. Lisowski, T. Klimczuk, A. Mikolajczyk and A. Zaleska-Medynska, *Appl. Catal., B*, 2022, **310**, 121349.
- 28 X. Huang, S. Yan, D. Deng, L. Zhang, R. Liu and Y. Lv, *ACS Appl. Mater. Interfaces*, 2021, **13**(2), 3471–3480.
- 29 W. G. Cui, Y. T. Li, H. Zhang, Z. C. Wei, B. H. Gao, J. J. Dai and T. L. Hu, *Appl. Catal., B*, 2020, **278**, 119262.
- 30 A. Ringaci, A. V. Yaremenko, K. G. Shevchenko, S. D. Zvereva and M. P. Nikitin, *Chem. Eng. J.*, 2021, **418**, 129386.
- 31 S. K. Elsaidi, M. A. Sinnwell, D. Banerjee, A. Devaraj, R. K. Kukkadapu, T. C. Droubay, Z. Nie, L. Kovarik, M. Vijayakumar, S. Manandhar and M. Nandasiri, *Nano Lett.*, 2017, **17**(11), 6968–6973.
- 32 L. Wang, C. Li, R. Wang, Y. Lin, K. Xiong, B. Wang and C. Hao, *J. Mol. Liq.*, 2023, **376**, 121373.
- 33 Y. Li, W. S. Lo, F. Zhang, X. Si, L. Y. Chou, X. Y. Liu, B. P. Williams, Y. H. Li, S. H. Jung, Y. S. Hsu and F. S. Liao, *J. Am. Chem. Soc.*, 2021, **143**(13), 5182–5190.
- 34 Y. Long, S. Song, J. Li, L. Wu, Q. Wang, Y. Liu, R. Jin and H. Zhang, *ACS Catal.*, 2018, **8**(9), 8506–8512.
- 35 Y. Zhang, M. Gutiérrez, A. K. Chaudhari and J. C. Tan, *ACS Appl. Mater. Interfaces*, 2020, **12**(33), 37477–37488.
- 36 C. H. Li, C. L. Huang, X. F. Chuah, D. S. Raja, C. T. Hsieh and S. Y. Lu, *Chem. Eng. J.*, 2019, **361**, 660–670.
- 37 E. H. Kwon, M. Kim, C. Y. Lee, M. Kim and Y. D. Park, *ACS Appl. Mater. Interfaces*, 2022, **14**(8), 10637–10647.
- 38 L. He, Y. Liu, J. Liu, Y. Xiong, J. Zheng, Y. Liu and Z. Tang, *Angew. Chem., Int. Ed.*, 2013, **52**(13), 3741–3745.
- 39 Y. Zhang, Y. Hu, G. Li and R. Zhang, *Mikrochim. Acta*, 2019, **186**, 1.
- 40 M. Zeng, Z. Chai, X. Deng, Q. Li, S. Feng, J. Wang and D. Xu, *Nano Res.*, 2016, **9**, 2729–2734.
- 41 C. Hou, L. Fu, Y. Wang, W. Chen, F. Chen, S. Zhang and J. Wang, *Cellulose*, 2021, **28**(14), 9253–9268.
- 42 C. L. Whitford, C. J. Stephenson, D. A. Gomez-Gualdrón, J. T. Hupp, O. K. Farha, R. Q. Snurr and P. C. Stair, *J. Phys. Chem. C*, 2017, **121**(45), 25079–25091.
- 43 P. Pachfule, X. Yang, Q. L. Zhu, N. Tsumori, T. Uchida and Q. Xu, *J. Mater. Chem. A*, 2017, **5**(10), 4835–4841.
- 44 X. Ma, J. Zhang, C. Zhang, X. Yang, A. Yu, Y. Huang, S. Zhang and G. Ouyang, *ACS Appl. Mater. Interfaces*, 2021, **13**(33), 40070–40078.
- 45 L. U. Zhang, Z. Wang, Y. Zhang, F. Cao, K. Dong, J. Ren and X. Qu, *ACS Nano*, 2018, **12**(10), 10201–10211.
- 46 J. Wan, Z. Zhao, H. Shang, B. Peng, W. Chen, J. Pei, L. Zheng, J. Dong, R. Cao, R. Sarangi and Z. Jiang, *J. Am. Chem. Soc.*, 2020, **142**(18), 8431–8439.
- 47 D. Li, X. Cao, Q. Zhang, X. Ren, L. Jiang, D. Li, W. Deng and H. Liu, *J. Mater. Chem. A*, 2019, **7**(23), 14108–14117.
- 48 Y. Liu, C. S. Gong, L. Lin, Z. Zhou, Y. Liu, Z. Yang, Z. Shen, G. Yu, Z. Wang, S. Wang and Y. Ma, *Theranostics*, 2019, **9**(10), 2791.
- 49 C. Yao, Q. Wang, C. Peng, R. Wang, J. Liu, N. Tsidaeva and W. Wang, *Chem. Eng. J.*, 2024, **479**, 147924.
- 50 Z. Wang, J. Niu, C. Zhao, X. Wang, J. Ren and X. Qu, *Angew. Chem.*, 2021, **133**(22), 12539–12545.
- 51 W. Zhu, G. Xiang, J. Shang, J. Guo, B. Motevalli, P. Durfee, J. O. Agola, E. N. Coker and C. J. Brinker, *Adv. Funct. Mater.*, 2018, **28**(16), 1705274.
- 52 X. Yang, S. Yuan, L. Zou, H. Drake, Y. Zhang, J. Qin, A. Alsalmeh and H. C. Zhou, *Angew. Chem.*, 2018, **130**(15), 3991–3996.
- 53 C. Li, M. Zhang, X. Di, D. Yin, W. Li and C. Liang, *Chin. J. Catal.*, 2016, **37**(9), 1555–1561.
- 54 D. Xu, Y. Qin, X. Cao, Y. Huang, J. Wang, X. Liu, F. Liu and X. Li, *Colloids Surf., A*, 2024, **696**, 134306.
- 55 T. Si, X. Lu, H. Zhang, S. Wang, X. Liang and Y. Guo, *Chin. Chem. Lett.*, 2022, **33**(8), 3869–3872.
- 56 D. Kim, G. Lee, S. Oh and M. Oh, *Chem. Commun.*, 2019, **55**(1), 43–46.
- 57 X. Gu, C. Huang, Z. Xu, H. Wu, R. Dong, R. Liu, J. Chen and H. Zhu, *J. Solid State Chem.*, 2021, **294**, 121803.



- 58 Y. Zhou, B. Tang, S. Wang and J. Long, *Int. J. Hydrogen Energy*, 2020, **45**(32), 15785–15795.
- 59 G. Lee, S. Lee, S. Oh, D. Kim and M. Oh, *J. Am. Chem. Soc.*, 2020, **142**(6), 3042–3049.
- 60 P. Á. Szilágyi, M. Lutz, J. Gascon, J. Juan-Alcañiz, J. Van Esch, F. Kapteijn, H. Geerlings, B. Dam and R. Van De Krol, *CrystEngComm*, 2013, **15**(30), 6003–6008.
- 61 M. X. Wu, Y. Wang, G. Zhou and X. Liu, *ACS Appl. Mater. Interfaces*, 2020, **12**(49), 54285–54305.
- 62 C. Dong, R. Tian, Y. Zhang, K. Liu, G. Chen, H. Guan and Z. Yin, *Chem. Eng. J.*, 2022, **442**, 136094.
- 63 H. Li, F. Yue, H. Xie, C. Yang, Y. Zhang, L. Zhang and J. Wang, *CrystEngComm*, 2018, **20**(7), 889–895.
- 64 S. J. Yin, H. Chen, S. Wang, Y. Wang and F. Q. Yang, *Heliyon*, 2023, **9**(5), 16245.
- 65 M. X. Wu, C. Wei, X. H. Wang, Q. Q. Xia, H. Wang and X. Liu, *Inorg. Chem.*, 2022, **61**(11), 4705–4713.
- 66 A. E. Abdelmaoula, J. Shu, Y. Cheng, L. Xu, G. Zhang, Y. Xia, M. Tahir, P. Wu and L. Mai, *Small Methods*, 2021, **5**(8), 2100508.
- 67 Q. Zhang, L. Fan, W. Liu, Y. Xie, J. Li and G. Huang, *J. Ind. Eng. Chem.*, 2023, **124**, 311–322.
- 68 M. Lu, Y. Deng, Y. Li, T. Li, J. Xu, S. W. Chen and J. Wang, *Anal. Chim. Acta*, 2020, **1110**, 35–43.
- 69 Y. Zhang, B. Wei and H. Liang, *ACS Appl. Mater. Interfaces*, 2023, **15**(2), 3442–3454.
- 70 C. Guo, J. Guo, Y. Zhang, D. Wang, L. Zhang, Y. Guo, W. Ma and J. Wang, *CrystEngComm*, 2018, **20**(47), 7659–7665.
- 71 K. Li, Y. Zhang, P. Wang, X. Long, L. Zheng, G. Liu, X. He and J. Qiu, *J. Alloys Compd.*, 2022, **903**, 163701.
- 72 H. Park, S. Oh, S. Lee, S. Choi and M. Oh, *Appl. Catal., B*, 2019, **246**, 322–329.
- 73 D. Li, X. Cheng, R. Xu, Y. Wu, X. Zhou, C. Ma and Y. Yu, *J. Mater. Chem. A*, 2019, **7**(34), 19929–19938.
- 74 L. Zhang, J. Wang, X. Ren, W. Zhang, T. Zhang, X. Liu, T. Du, T. Li and J. Wang, *J. Mater. Chem. A*, 2018, **6**(42), 21029–21038.
- 75 Y. Liu, C. Wu, Z. Zhou, W. Liu, H. Guo and B. Zhang, *J. Membr. Sci.*, 2022, **659**, 120787.
- 76 H. Tan, X. Zhao, L. Du, B. Wang, Y. Huang, Y. Gu and Z. Lu, *Small*, 2024, **20**(3), 2305881.
- 77 S. R. Hosseini, M. Omidkhan, Z. M. Lighvan, S. Norouzbahari and A. Ghadimi, *Sep. Purif. Technol.*, 2023, **307**, 122679.
- 78 Z. Zhao, J. Ding, R. Zhu and H. Pang, *J. Mater. Chem. A*, 2019, **7**(26), 15519–15540.
- 79 W. Zhan, Q. Kuang, J. Zhou, X. Kong, Z. Xie and L. Zheng, *J. Am. Chem. Soc.*, 2013, **135**(5), 1926–1933.
- 80 X. Zhang, Q. Han and M. Ding, *RSC Adv.*, 2015, **5**(2), 1043–1050.
- 81 R. Chen, C. Tao, Z. Zhang, X. Chen, Z. Liu and J. Wang, *ACS Appl. Mater. Interfaces*, 2019, **11**(46), 43156–43165.
- 82 J. Zhuang, L. Y. Chou, B. T. Sneed, Y. Cao, P. Hu, L. Feng and C. K. Tsung, *Small*, 2015, **11**(41), 5551–5555.
- 83 C. Guo, J. Guo, Y. Zhang, D. Wang, L. Zhang, Y. Guo, W. Ma and J. Wang, *CrystEngComm*, 2018, **20**, 7659–7665.
- 84 H. Wang, X. Yuan, Y. Wu, G. Zeng, H. Dong, X. Chen, L. Leng, Z. Wu and L. Peng, *Appl. Catal., B*, 2016, **186**, 19–29.
- 85 F. Meng, S. Zhang, L. Ma, W. Zhang, M. Li, T. Wu, H. Li, T. Zhang, X. Lu, F. Huo and J. Lu, *Adv. Mater.*, 2018, **30**(49), 1803263.
- 86 S. Ding, J. Wan, Y. Ma, Y. Wang, M. Pu, X. Li and J. Sun, *J. Hazard. Mater.*, 2021, **411**, 125194.
- 87 W. Bao, M. Liu, J. Meng, S. Liu, S. Wang, R. Jia, Y. Wang, G. Ma, W. Wei and Z. Tian, *Nat. Commun.*, 2021, **12**(1), 6399.
- 88 X. Meng, J. Deng, F. Liu, T. Guo, M. Liu, P. Dai, A. Fan, Z. Wang and Y. Zhao, *Nano Lett.*, 2019, **19**(11), 7866–7876.
- 89 L. Zhang, J. Zhang, X. Li, C. Wang, A. Yu, S. Zhang, G. Ouyang and Y. Cui, *Appl. Surf. Sci.*, 2021, **538**, 148054.
- 90 D. Lin, P. Duan, W. Yang, Y. Liu and Q. Pan, *Inorg. Chem. Front.*, 2020, **7**, 1643–1650.
- 91 S. Ehrling, C. Kutzscher, P. Freund, P. Müller, I. Senkovska and S. Kaskel, *Microporous Mesoporous Mater.*, 2018, **263**, 268–274.
- 92 S. Furukawa, K. Hirai, K. Nakagawa, Y. Takashima, R. Matsuda, T. Tsuruoka, M. Kondo, R. Haruki, D. Tanaka, H. Sakamoto and S. Shimomura, *Angew. Chem.*, 2009, **121**(10), 1798–1802.
- 93 C. Guo, F. Duan, S. Zhang, L. He, M. Wang, J. Chen, J. Zhang, Q. Jia, Z. Zhang and M. Du, *J. Mater. Chem.*, 2022, **10**(2), 475–507.
- 94 M. X. Wu, Y. Wang, G. Zhou and X. Liu, *ACS Appl. Mater. Interfaces*, 2020, **12**(49), 54285–54305.
- 95 C. Liu, J. Wang, J. Wan and C. Yu, *Coord. Chem. Rev.*, 2021, **432**, 213743.
- 96 Y. Shan, L. Chen, H. Pang and Q. Xu, *Small Struct.*, 2021, **2**(2), 2000078.
- 97 X. Yang, S. Yuan, L. Zou, H. Drake, Y. Zhang, J. Qin, A. Alsalmeh and H. C. Zhou, *Angew. Chem.*, 2018, **130**(15), 3991–3996.
- 98 M. Liu, Z. Xing, Z. Li and W. Zhou, *Coord. Chem. Rev.*, 2021, **446**, 214123.
- 99 W. Guo, W. Xia, K. Cai, Y. Wu, B. Qiu, Z. Liang, C. Qu and R. Zou, *Small*, 2017, **13**(41), 1702049.
- 100 L. Figueroa-Quintero, D. Villalgorido-Hernández, J. J. Delgado-Marín, J. Narciso, V. K. Velisoju, P. Castaño, J. Gascón and E. V. Ramos-Fernández, *Small Methods*, 2023, **7**(4), 2201413.
- 101 X. Song, T. K. Kim, H. Kim, D. Kim, S. Jeong, H. R. Moon and M. S. Lah, *Chem. Mater.*, 2012, **24**(15), 3065–3073.
- 102 J. A. Boissonnault, A. G. Wong-Foy and A. J. Matzger, *ACS Appl. Mater. Interfaces*, 2017, **139**(42), 14841–14844.
- 103 Y. Gu, Y. Wu, L. Li, W. Chen, F. Li and S. Kitagawa, *Angew. Chem., Int. Ed.*, 2017, **129**(49), 15864–15868.
- 104 J. Zhuang, L. Y. Chou, B. T. Sneed, Y. Cao, P. Hu, L. Feng and C. K. Tsung, *Small*, 2015, **11**, 5551–5555.
- 105 L. Feng, S. Yuan, J. L. Li, K. Y. Wang, G. S. Day, P. Zhang, Y. Wang and H. C. Zhou, *ACS Cent. Sci.*, 2018, **4**, 1719–1726.
- 106 P. Gao, Y. Chen, W. Pan, N. Li, Z. Liu and B. Tang, *Angew. Chem., Int. Ed.*, 2021, **133**(31), 16901–16914.
- 107 M. Nazari, A. S. Saljooghi, M. Ramezani, M. Alibolandi and M. Mirzaei, *J. Mater. Chem. B*, 2022, **10**(43), 8824–8851.
- 108 R. Weissleder and M. Nahrendorf, *Proc. Natl. Acad. Sci. U. S. A.*, 2015, **112**(47), 14424–14428.
- 109 H. S. Wang, *Coord. Chem. Rev.*, 2017, **349**, 139–155.



- 110 L. Zhang, M. Liu, Z. Fang and Q. Ju, *Coord. Chem. Rev.*, 2022, **468**, 214641.
- 111 L. Zhang, C. Liu, Y. Gao, Z. Li, J. Xing, W. Ren, L. Zhang, A. Li, G. Lu, A. Wu and L. Zeng, *Adv. Healthcare Mater.*, 2018, **7**(24), 1870086.
- 112 H. X. Zhao, Q. Zou, S. K. Sun, C. Yu, X. Zhang, R. J. Li and Y. Y. Fu, *Chem. Sci.*, 2016, **7**(8), 5294–5301.
- 113 T. Wang, S. Li, Z. Zou, L. Hai, X. Yang, X. Jia, A. Zhang, D. He, X. He and K. Wang, *J. Mater. Chem. B*, 2018, **6**(23), 3914–3921.
- 114 X. Zheng, L. Wang, Y. Guan, Q. Pei, J. Jiang and Z. Xie, *Biomaterials*, 2020, **235**, 119792.
- 115 H. Alijani, A. Noori, N. Faridi, S. Z. Bathaie and M. F. Mousavi, *J. Solid State Chem.*, 2020, **292**, 121680.
- 116 Y. Wang, K. Liu, M. Zhang, T. Xu, H. Du, B. Pang and C. Si, *Carbohydr. Polym.*, 2023, **313**, 120851.
- 117 Y. Cui, J. Zhang, H. He and G. Qian, *Coord. Chem. Rev.*, 2018, **47**(15), 5740–5785.
- 118 E. Dezhakam, R. F. Vayghan, S. Dehghani, T. Kafili-Hajlari, A. Naseri, M. Dadashpour, B. Khalilzadeh and G. S. Kanberoglu, *Sci. Rep.*, 2024, **14**(1), 29850.
- 119 S. Khan, W. C. Cho, A. Sepahvand, S. Haji Hosseinali, A. Hussain, M. M. Nejadi Babadaei, M. Sharifi, M. Falahati, L. A. Jaragh-Alhadad, T. L. Ten Hagen and X. Li, *J. Nanobiotechnol.*, 2023, **21**(1), 136.
- 120 T. Liu, R. Zhou, C. Zhang, Y. Yi and G. Zhu, *Chem. Commun.*, 2023, **59**(25), 3771–3774.
- 121 M. Lu, Y. Deng, Y. Li, T. Li, J. Xu, S. W. Chen and J. Wang, *Anal. Chim. Acta*, 2020, **1110**, 35–43.
- 122 R. Taheri-Ledari, S. Zarei-Shokat, F. S. Qazi, M. Ghafori-Gorab, F. Ganjali, A. Kashtiaray, M. Mahdavi, M. Safavi and A. Maleki, *ACS Appl. Mater. Interfaces*, 2023, **17**(12), 17703–17717.
- 123 L. He, K. Pang, W. Liu, Y. Tian, L. Chang, X. Liu, M. Zhao, Y. Liu, Y. Li, X. Jiang and R. Song, *J. Mater. Chem. B*, 2019, **7**(7), 1050–1055.
- 124 X. Cai, Y. Zhao, L. Wang, M. Hu, Z. Wu, L. Liu, W. Zhu and R. Pei, *J. Mater. Chem. B*, 2021, **9**(33), 6646–6657.
- 125 X. Zhao, S. He, B. Li, B. Liu, Y. Shi, W. Cong, F. Gao, J. Li, F. Wang, K. Liu, C. Sheng, J. Su and H. G. Hu, *Nano Lett.*, 2023, **23**(3), 863–871.
- 126 T. C. Livesey, L. A. M. Mahmoud, M. G. Katsikogianni and S. Nayak, *Pharmaceutics*, 2023, **15**(1), 274.
- 127 L. Yan, A. Gopal, S. Kashif, P. Hazelton, M. Lan, W. Zhang and X. Chen, *Chem. Eng. J.*, 2022, **435**, 134975.
- 128 Y. Tu, C. Lei, F. Deng, Y. Chen, Y. Wang and Z. Zhang, *New J. Chem.*, 2021, **45**(19), 8701–8713.
- 129 K. Huang, F. Li, K. Yuan, Y. Yang, H. Chang, Y. Liang, X. Yan, J. Zhao, T. Tang and S. Yang, *Appl. Mater. Today*, 2022, **28**, 101513.
- 130 C. Liang, L. Xu, G. Song and Z. Liu, *Chem. Soc. Rev.*, 2016, **45**(22), 6250–6269.
- 131 Z. Bao, K. Li, P. Hou, R. Xiao, Y. Yuan and Z. Sun, *Mater. Chem. Front.*, 2021, **5**, 1632–1654.
- 132 Y. Zeng, G. Xu, X. Kong, G. Ye, J. Guo, C. Lu, A. Nezamzadeh-Ejhieh, M. S. Khan, J. Liu and Y. Peng, *Int. J. Pharm.*, 2022, **627**, 122228.
- 133 L. He, Q. Ni, J. Mu, W. Fan, L. Liu, Z. Wang, L. Li, W. Tang, Y. Liu, Y. Cheng and L. Tang, *J. Am. Chem. Soc.*, 2020, **142**(14), 6822–6832.
- 134 L. He, M. Brasino, C. Mao, S. Cho, W. Park, A. P. Goodwin and J. N. Cha, *Small*, 2017, **13**(24), 1700504.
- 135 Y. Shao, B. Liu, Z. Di, G. Zhang, L.-D. Sun, L. Li and C.-H. Yan, *ACS Appl. Mater. Interfaces*, 2020, **12**, 3939–3946.
- 136 K. Lu, C. He and W. Lin, *ACS Appl. Mater. Interfaces*, 2014, **136**(48), 16712–16715.
- 137 Q. Ding, Z. Xu, L. Zhou, C. Rao, W. Li, M. Muddassir, H. Sakiyama, B. Li, Q. Ouyang and J. Liu, *J. Colloid Interface Sci.*, 2022, **621**, 180–194.
- 138 X. Lin, H. Wu, J. Zhang, X. Chen, X. Gao and Y. Liu, *Chem. Eng. J.*, 2024, **480**, 147865.
- 139 X. Yang, S. Yuan, L. Zou, H. Drake, Y. Zhang, J. Qin, A. Alsalmeh and H. C. Zhou, *Angew. Chem., Int. Ed.*, 2018, **130**(15), 3991–3996.
- 140 S. Z. Ren, B. Wang, X. H. Zhu, D. Zhu, M. Liu, S. K. Li, Y. S. Yang, Z. C. Wang and H. L. Zhu, *ACS Appl. Mater. Interfaces*, 2020, **12**(22), 24662–24674.
- 141 S. Khan, M. Falahati, W. C. Cho, Y. Vahdani, R. Siddique, M. Sharifi, L. A. Jaragh-Alhadad, S. Haghghat, X. Zhang, T. L. Ten Hagen and Q. Bai, *Adv. Colloid Interface Sci.*, 2023, **321**, 103007.
- 142 Z. Wang, W. Yu, N. Yu, X. Li, Y. Feng, P. Geng, M. Wen, M. Li, H. Zhang and Z. Chen, *Chem. Eng. J.*, 2020, **400**, 125877.
- 143 S. Li, X. Shi, H. Wang and L. Xiao, *J. Biomed. Mater. Res., Part B*, 2021, **109**(6), 841–852.
- 144 J. Liu, T. Liu, P. Du, L. Zhang and J. Lei, *Angew. Chem., Int. Ed.*, 2019, **58**, 7808–7812.
- 145 Z. Zhou, J. Zhao, Z. Di, B. Liu, Z. Li, X. Wu and L. Li, *Nanoscale*, 2021, **13**(1), 131–137.
- 146 S. Rojas, A. Arenas-Vivo and P. Horcajada, *Coord. Chem. Rev.*, 2019, **388**, 202–226.
- 147 J. Y. Zeng, M. K. Zhang, M. Y. Peng, D. Gong and X. Z. Zhang, *Adv. Funct. Mater.*, 2018, **28**(8), 1705451.
- 148 L. He, N. Zheng, Q. Wang, J. Du, S. Wang, Z. Cao, Z. Wang, G. Chen, J. Mu, S. Liu and X. Chen, *Adv. Sci.*, 2023, **10**(1), 2205208.

